



D1.31 Report on PI based assessment of reduced tower top mass concepts

Agreement n.:	308974
Duration	November 2012 – October 2017
Co-ordinator:	DTU Wind



The research leading to these results has received funding from the European Community's Seventh Framework Programme FP7-ENERGY-2012-1-2STAGE under grant agreement No. 308974 (INNWIND.EU).

PROPRIETARY RIGHTS STATEMENT

This document contains information, which is proprietary to the "INNWIND.EU" Consortium. Neither this document nor the information contained herein shall be used, duplicated or communicated by any means to any third party, in whole or in parts, except with prior written consent of the "INNWIND.EU" consortium.

Document information

Document Name:	Report on PI based assessment of reduced tower top mass concepts
Document Number:	Deliverable D 1.31
Author:	Dariusz Dabrowski, Anand Natarajan Bernard H. Bulder, Edwin T.G. Bot
Document Type	Report
Dissemination level	PU
Review:	Takis Chaviaropoulos
Date:	31-08-2015
WP:	WP 1
Task:	Task 1.3
Approval:	Approved by Project Coordinator

TABLE OF CONTENTS

TABLE OF CONTENTS	3
1 INTRODUCTION.....	5
1.1 Tower Top steel structure mass minimisation	5
1.2 Variable Axial Induction distribution along the rotor blade span	5
2 TOWER TOP STEEL STRUCTURE MASS MINIMISATION.....	7
2.1 Design concept of a 10 MW wind turbine nacelle	7
2.2 Topology optimisation	8
2.2.1 Finite element model	8
2.2.2 Topology optimisation	10
2.2.3 Verification with additional loads	14
2.3 Reduction of nacelle mass	15
2.3.1 New design of components	15
2.3.2 Comparison of proposed designs.....	18
2.4 Bolted connection between components	19
2.4.1 Flange connection	19
2.4.2 Two stud connection	22
2.5 Mass reduced tower top concept.....	23
2.6 Concept of a 20 MW Turbine.....	26
2.7 Conclusions	28
3 VARIABLE AXIAL INDUCTION DISTRIBUTION ALONG THE ROTOR SPAN.....	30
3.1 Concept description	30
3.2 Cost Model.....	31
3.2.1 The blade cost model.....	32
3.2.2 The tower cost model.....	33
3.3 Results.....	35
3.4 Conclusions	36

1 INTRODUCTION

This report is the deliverable D.1.31 about a performance indicator based assessment of reduced tower top mass concepts. The report is split in 2 sections. The first section deals with the tower top mass minimisation for a direct drive concept. The second section deals with a concept where it is investigated whether variable axial induction along the span of the rotor leads to lower blade masses and consequently lower loads in the drive train.

1.1 Tower Top steel structure mass minimisation

New designs for large wind turbines can decrease cost of the offshore wind farms, and thus the overall cost of the generated energy. For large wind turbine configurations of 10 MW and larger a direct drive presents a more compact solution over geared solutions. Furthermore if the generator is placed in front of the hub, a so called compact “king pin” solution is designed, see [1, 2]. This allows the generator to be coupled directly to the hub. In this study the detailed structural design of the 10 MW king pin drive and nacelle is made using extreme loads obtained from the 10 MW INN WIND.EU reference wind turbine.

The main objective of the presented study is to address the performance indicator of cost reduction by reducing the tower top steel structure mass of the down selected innovative wind turbine. Additionally, in the report, the ultimate design stresses of the wind turbine load carrying components are determined and two concepts of jointed connections are analysed.

1.2 Variable Axial Induction distribution along the rotor blade span

The idea behind this conceptual study is that by varying the axial induction along the span the load force distribution varies along the span and that by optimising that the weight of the rotor blades can be reduced. Lower weights of the rotor blades due to lower loading will influence the weights and cost of other components like the drive train & tower too.

For this concept it is required to use and adapt a simple engineering cost model of the blade where the blade loads are calculated with an approximate model that is tuned for the reference wind turbine rotor blade. Next to that an estimate is made what the influence will be for the tower and drive train. The results of these analyses will be applied in the INN WIND.EU cost model D1.23

The blade weights of the rotor with different axial induction factors is compared and multiplied with an indicative cost of the blade, in the INN WIND.EU cost model to show the effect on the LCoE.

2 TOWER TOP STEEL STRUCTURE MASS MINIMISATION

2.1 Design concept of a 10 MW wind turbine nacelle

An innovative design concept of 10 MW wind turbine nacelle with 178 m rotor diameter was proposed in deliverable D3.42 wherein a 10 MW superconducting direct drive generator was integrated in the front of turbine rotor. This nacelle concept is based on the king-pin and mounted in the front of rotor blades. In figure 1, a view on the turbine nacelle is presented.

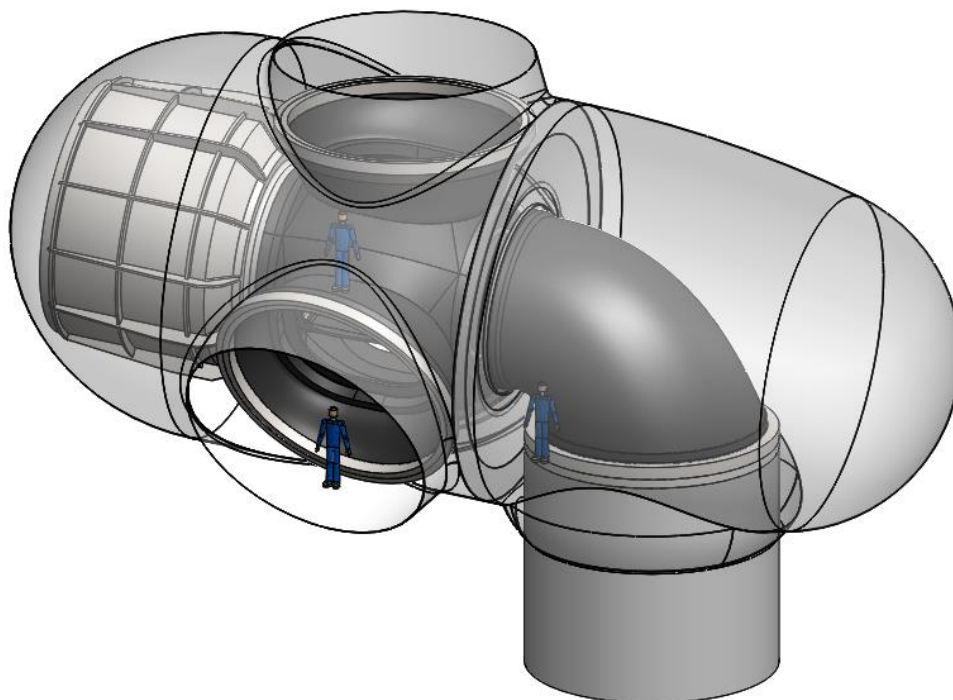


Figure 1 10 MW direct drive wind turbine

Key features of presented design of turbine are generator mounted in front of the rotor blades and king-pin nacelle layout. In figure 2, a detailed view of the turbine nacelle is presented.

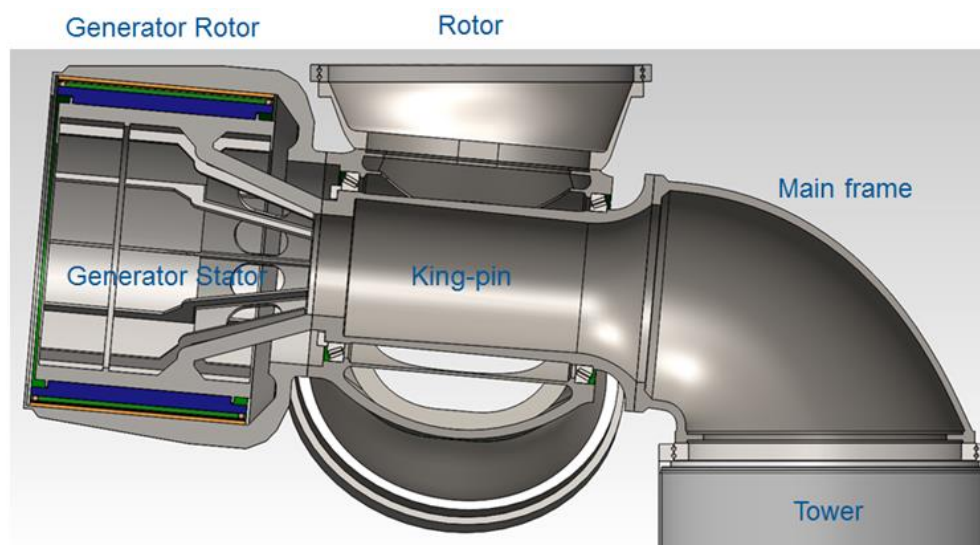


Figure 2 King-pin nacelle layout (Based on D3.42)

In the assembly presented above the rotor is supported by two bearings, upwind and downwind, on the king-pin. The king-pin is fixed to the mainframe, which is connected by the yaw bearing with the tower. On the upwind side of the king-pin is connected the generator stator. The rotor with generator rotor rotates relative to the generator stator, which is fixed to the king-pin. The design in figure 1 is conceptual and further refinements are required in terms of jointed connections between the mainframe and the king-pin, generator and king-pin and avoidance of stress concentration regions.

In this report, a stress analysis by application of finite element method is done to ensure the structural integrity of the innovative nacelle and a structural optimization is done with compliance limits to minimize the mass of the nacelle assembly. Analysis of stress distribution on the drive train components allows to verify safety of the design and to determine areas that can be removed to reduce the structural mass of the nacelle.

2.2 Topology optimisation

2.2.1 Finite element model

From the geometry of the direct drive nacelle construction, the load carrying sections from the rotor of the generator to the tower are analysed in the FE pre-processor Hypermesh [3] and solver Optistruct [4] from Altair to determine regions of stress concentration. All loads derived from the rotor and generator are transferred by the king-pin and mainframe to the tower. The loads comprising of the thrust, bending and torsional moments are the result of rotor interactions on the upwind and downwind bearings during wind turbine operations. The high stress concentration areas are caused mostly by sharp edges. In presented design few sharp edges on profile were found and modified by adding fillets or increasing existing fillets radius. The finite element model with constraints is presented in figure 3.

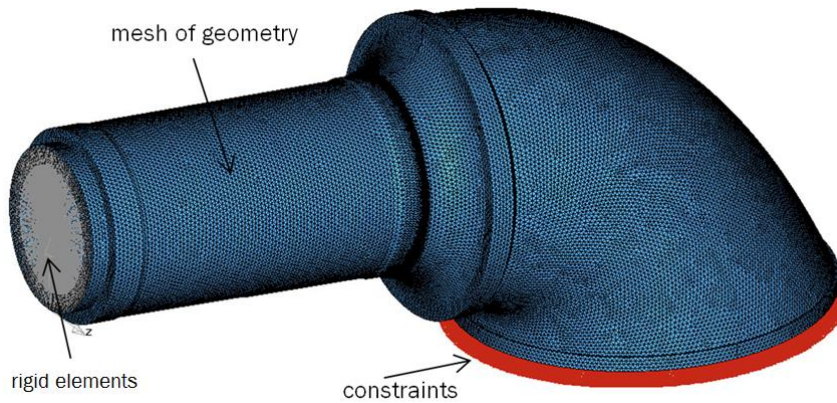


Figure 3 Finite element model with constraints

The FE model was built with 3D elements (tetrahedrons). To calculate stress distribution on the nacelle parts following loads, including safety factors, were applied: bending moment from rotor 18300 kNm, thrust force 4600 kN and torsional moment from generator with value of 16500 kNm. The torsional moment from generator was applied on the king-pin in connection area with generator stator using 1D rigid elements. The thrust force was applied on the surface vertical to the rotor axis in the downwind bearing support. The bending moment derived from bearings forces was applied as a pressure on the bearings support surfaces. Applied forces were estimated on the basis of ultimate loads obtained from HAWC2 simulations for 10 MW DTU reference wind turbine [5]. The simulations were conducted for DLC 1.3 from IEC 61400-1, which was the critical case for extremes. The nacelle design should also be verified in terms of the fatigue damage, but this can be performed in the next stage in Task 3.4 since detailed analysis of DLC 1.2 is required which is not possible at the present stage. The model was constrained on the bottom part of the mainframe. The stress simulation results are presented in figure 4.

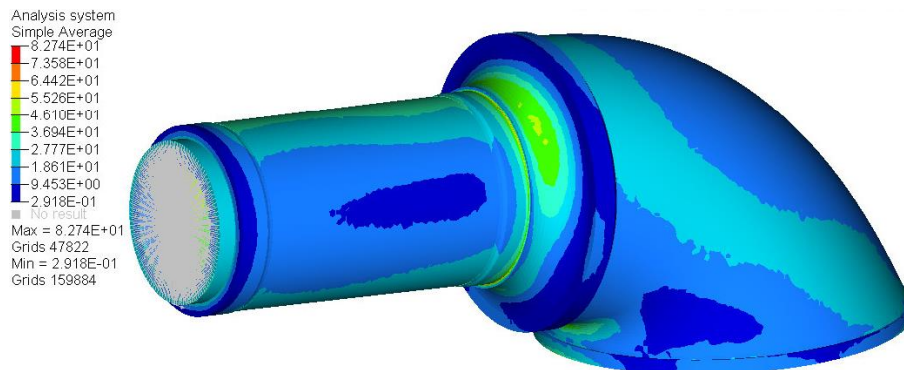


Figure 4 Von Mises stress distributions in nacelle components [MPa]

From FE analysis it is visible that von Mises stress in the mainframe are concentrated in the bottom part but for the king-pin element they are mostly focused in the upper part of the flange and in the downwind bearing support.

On the basis of presented analysis it was shown that there are high stress concentration points in the structure but also there are several areas on the components that have low stress values, so it is proposed to reduce mass in these areas by application of structural optimization methods.

2.2.2 Topology optimisation

The weight and mechanical properties of wind turbine parts depend on material and manufacturing techniques. Only suitable materials with proper strength properties in a specified working environment can be used for wind turbine load transmitting components. The choice of material shall be related to the demands to be made on the component, particularly the type of load as well as the external conditions and to the design [6]. The nacelle usually relates to 25 to 40% of the total weight of wind turbines [7]. It contains the drivetrain components and the other equipment like anemometer, brakes, controller, convertor, cooling system, sensors, and yaw drive system. Materials used for these components are primarily cast iron, steel, aluminium, copper, plastic and stainless steel [8].

On the basis of GL Guidelines for the Certification of Wind Turbines [6] a mainframe and drivetrain components can be made from structural steels, cast steel, forging steel and cast iron. The characteristic values of used materials shall be taken from the corresponding standards. In the report, two main load carrying parts of the concept direct drive wind turbine are analysed; the mainframe and king-pin. Manufacturing of these parts is usually casting. In table 1 comparison of prices for cast irons and cast steels are presented.

Table 1. Comparison of material prices [9]

Material	Description	Approximate Price
Grey cast iron	Casting parts with low tensile strength	1.50 USD/kg
Ductile cast iron	Casting parts with high tensile strength	1.67 USD/kg
Cast steel	Not complex structure, normal surface quality	1.37 USD/kg
Cast steel	Complex structure, good surface quality	2.42 USD/kg

* prices valid on 22.07.2015

The cast iron usually refers to grey iron, ductile iron and malleable iron, which is iron casting with carbon content upper than 2 %, and cast steel usually, refers to normal carbon steel and alloy steel, or called steel casting with carbon content lower than 2 % [10]. The advantage of cast steel are good mechanical properties, design flexibility, high tensile stress or dynamic load, and disadvantage are low wear resistance, mobility weight and the casting performance are compared bad with cast iron and the costs are usually higher than normal cast iron [10]. Grey cast iron has good casting properties, vibration damping, wear resistance, and good machinability. However, its tensile strength and elongation are very low. The ductile iron and malleable iron have high strength, ductility, heat-resistance and toughness, so it can be used in a wider applications, in some cases can replace the carbon steel but the production cost is higher [10]. In table 2 ductile and grey cast iron properties are listed.

Table 2. Cast iron properties [9]

Material	Standard	Symbol	Tensile strength
Gray cast iron	ASTM A48	EN-GJL-150	150 MPa
	ASTM A48	EN-GJL-200	200 MPa
Ductile cast iron	ASTM A536	EN-GJS-350	320 MPa
	ASTM A536	EN-GJS-400	370 MPa

* Tensile strength for wall thickness more than 100 mm

In the study, the mainframe and king-pin are made from ductile cast iron EN-GJS-400 [7, 11, 12], but other component like bolts are made from steel. For chosen material the tensile strength is 370 MPa, what corresponds to the yield strength of 296 MPa. The safety factor for material strength was assumed 1.2, which gives design strength for material 246 MPa.

The goal of the study is to propose a lightweight design for the mainframe and king-pin with predefined stiffness, for this reason topology optimization was conducted. In the study, requirements for bolts connecting the parts are taken into account. Topology optimization is a technique to find the optimal layout of a structure within a specified design domain and is an iterative process in which the material is removed or re-distributed from the initial domain. The sensitivity in topology optimization has to be analysed to characterize the change of the objective function due to changes in design variables [12, 13]. In the study, finite element model described in the previous chapter was used and the optimization domain was assumed on the mainframe between flange and yaw bearing. The finite element model with design area marked with red colour is presented in figure 5.

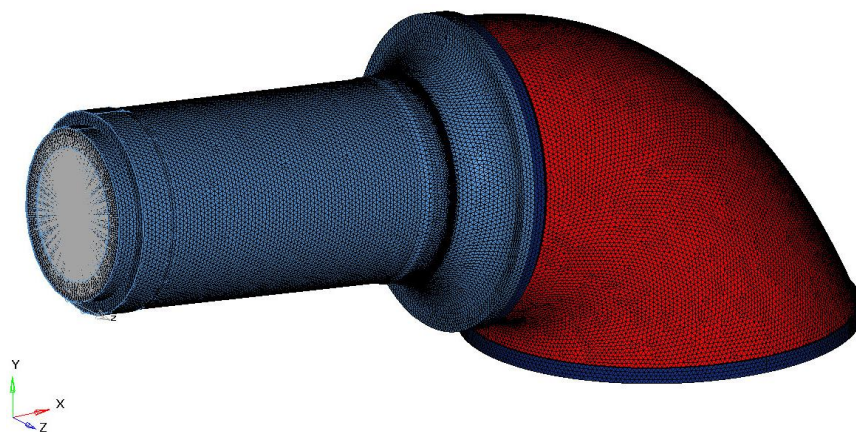


Figure 5 Finite element model and design area (red) for topology optimization

The optimization is performed on the mainframe, which from the downwind side is mounted to the tower top yaw bearing and from the upwind side to the generator. In the topology optimization problem the design variable is density of finite elements, objective is to minimize volume of the design area and constraint is displacement of nodes on the upwind side of the king-pin. For optimization the Optistruct solver [4] was used. The optimization problem in the solver is solved by gradient-based optimization which uses gradient values to find a minimum of an objective function. In optimization the local approximation method is used, which is an iterative procedure which assumes that the biggest changes in the design occur in the first few optimization steps and small changes in each further optimization steps [4]. Optistruct optimizer has implemented three different algorithms: the optimality criteria method, dual method, and primal feasible directions method [4]. In common topology optimization case where the number of design variables exceeds the number of constraints dual method is used [4, 14]. The dual method is a mathematical programming method designed for solving structural optimization problems [15]. The method employs mixed design variables (direct or reciprocal) to get first-order approximations to the objective function and constraints. The main advantage of this method is inherent tendency to generate a sequence of steadily improving feasible designs [15].

The stiffness of lightweight structure was assumed to be close to the primary design under applied loads. The maximum displacement in FE analysis presented in previous chapter was recorded on the nodes connecting the king-pin with generator, and it was 6 mm in magnitude. In further study three topology optimization cases will be presented, in which different value of displacement constraint were assumed: 15 mm, 20 mm and 30 mm. The selected constraints have relatively low values with comparison to the components dimensions. It is so as to not to interfere significantly on the clearance between the rotor and tower and design requirements for other

components in the wind turbine. In the analysis the manufacturing constraints used, are symmetry of the design on the rotor axis and minimum membrane size higher than 360 mm. These constraints allow the solver to obtain reasonable geometry of parts for casting.

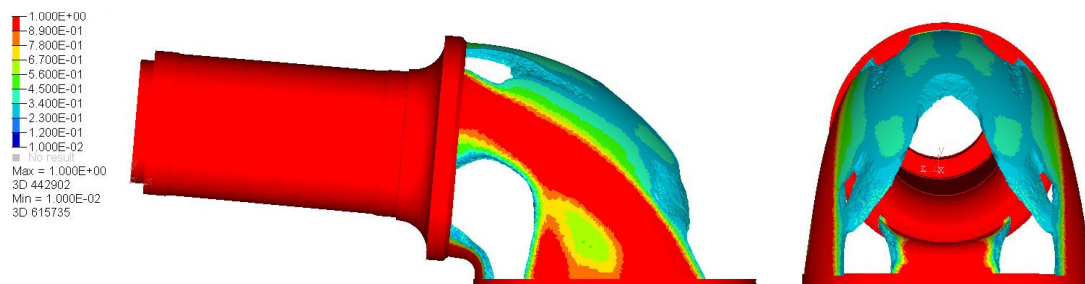


Figure 6 Topology optimization results for displacement constraint 15 mm and element density more than 0.3

In presented topology optimization analysis design variable is the density of finite elements used in the model, in figure 6 results of optimization are presented for elements density higher than 0.3. In this optimization case displacement constraint of 15 mm on nodes on upwind side of the king-pin (connection surface between generator and king-pin) were assumed. The solver for presented problem is converging in few iterations and leads to a feasible design. Presented results can serve as an input for a new design of the mainframe, in which mass can be reduced from the side parts and bottom back of the component. In figure 7, the ultimate stress distribution in the analysed components after optimization is presented.

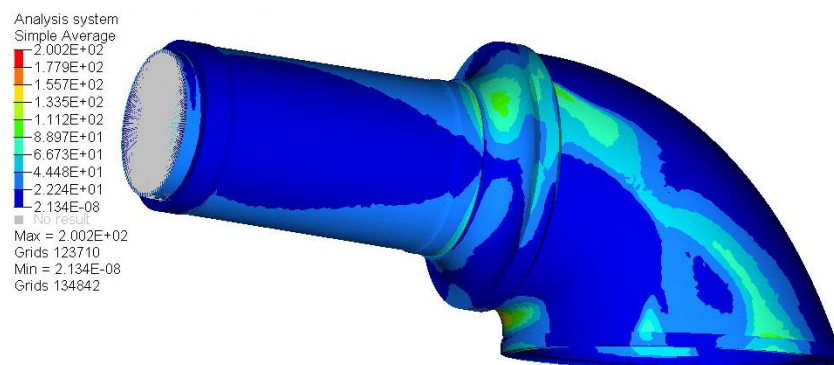


Figure 7 Von Mises stress distributions in components after optimization [MPa] (displacement constraint 15 mm)

After topology optimization, the material density of the elements within the design domain has been changed, which causes changes in the distribution of stresses in the mainframe. In the new model stresses are mostly distributed on sides and bottom front part of the mainframe and the maximum von Mises stress is 200 MPa. In the next presented case, the displacement constraint on the upwind side of the king-pin was assumed 20 mm and the same manufacturing constraints as before are retained.

In this case the optimization converges after 24 iterations and a feasible design was obtained within the prescribed constraints. In figure 8, the topology optimization results for element density are presented, where the element density is higher than 0.3. The element density is the material density within each Finite Element. The results in Fig. 8 present further mass reduction.

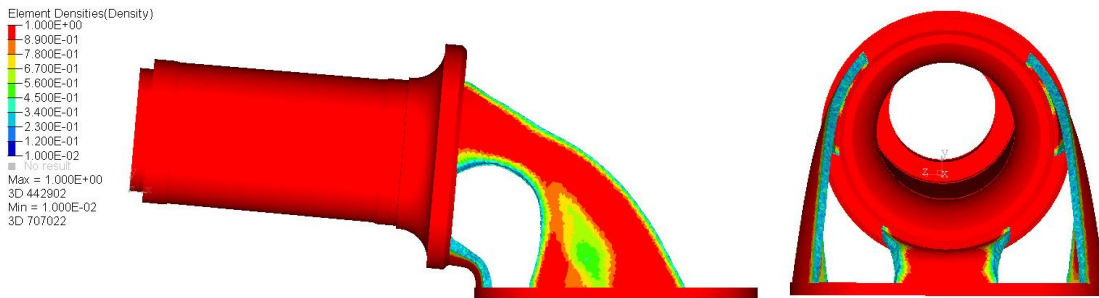


Figure 8 Topology optimization results for displacement constraint 20 mm and element density more than 0.3

Analysing front and back views of the model after optimization one can see that a significant amount of weight has been reduced in the mainframe by removing material from back and side parts. This weight reduction also will affect the stiffness of the component and results in higher ultimate stress values as presented in figure below.

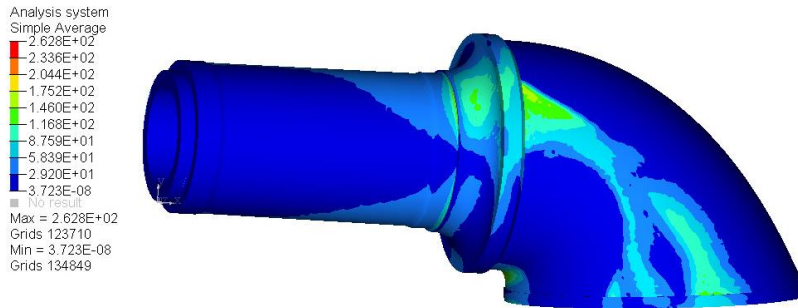


Figure 9 Von Mises stress distributions in components after optimization [MPa] (displacement constraint 20 mm)

The von Mises stress in components after optimization for displacement constraint 20 mm is higher than design value. The maximum value of stresses is 262 MPa what is 62 MPa higher than in the previous example. In the last optimization case the displacement constraint in the same location as previously was relaxed further as to not exceed 30 mm.

Constraint parameters in this case allow us to obtain the highest mass reduction in design area but the stiffness of components is at its lowest limit. The topology optimization is converging in 22 iterations. In figure 10 the analysis results are presented.

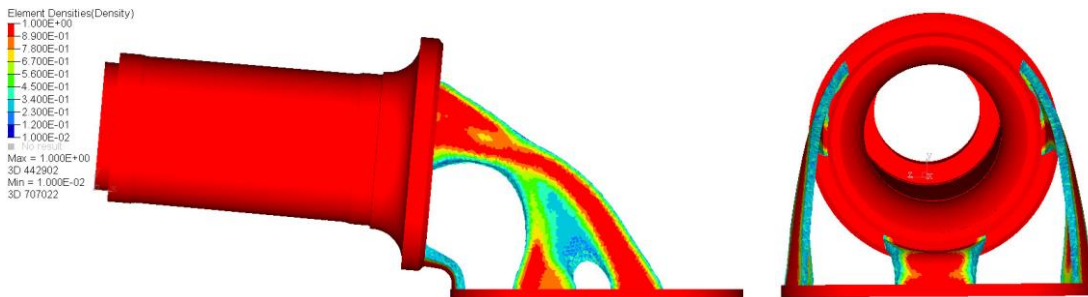


Figure 10 Topology optimization results for displacement constraint 30 mm and element density more than 0.3

The red area, which represents elements with highest density, in results plot has been decreased what provides higher mass reduction but on the other hand the ultimate stress values have been increased to a value of 310 MPa, what exceeds the safety limits, figure 11. The maximum load carrying points in this case are on the bottom part of the mainframe and on the upper side wall.

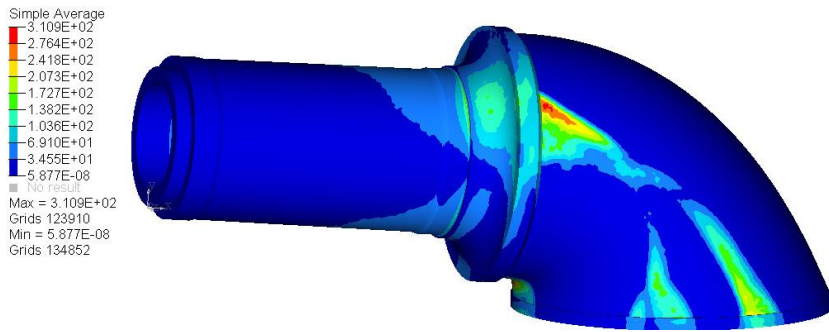


Figure 11 Von Mises stress distributions in components after optimization [MPa] (displacement constraint 30 mm)

2.2.3 Verification with additional loads

The loads introduced in the topology optimization presented above do not cover all spectrum of hub loads for a wind turbine, but only a subset of thrust, fore-aft bending moment and torsional moment. These loads do not include, weight of direct-drive generator and rotor since a conservative approach is used herein, as the moment from the vertical force is in the opposite direction of the fore-aft bending moment and thereby reduces the net moment. However the effect of the side-side bending moment is now included whereby in the topology optimization an additional load which is the side moment is also acting on the king-pin. The side moment was assumed 10000 kNm which is the coincidence moment for the extreme thrust, and was applied on bearings supports.

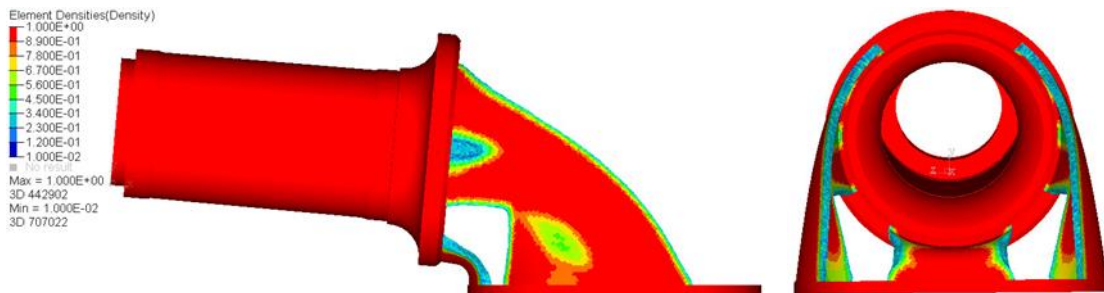


Figure 12 Topology optimization results for structure with side moment (displacement constraint 20 mm and element density more than 0.3)

In Figure 12, the optimization results are presented for additional load case. One can observe that topology is similar as for the results presented in figure 8, which represents analysis for the same stiffness of the structure (maximum deformation of 20 mm), except stronger side walls. In figure 13 distribution of von Mises stress after optimization is presented. Therefore the addition of the side-side moment does not change general topology obtained in previous optimization cases.

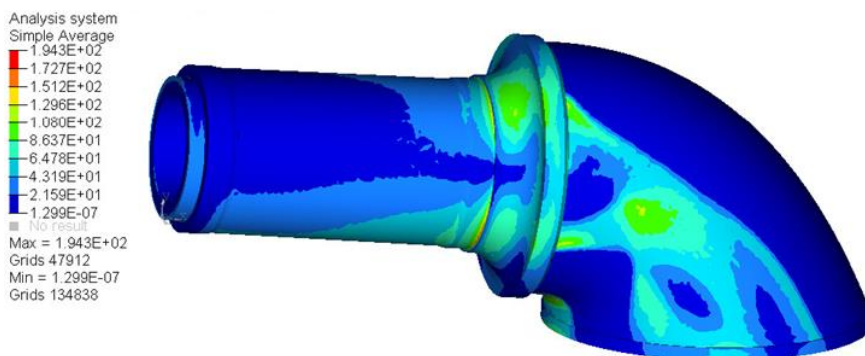


Figure 13 Von Mises stress distributions in components after optimization [MPa] (displacement constraint 20 mm)

To summarize, in this chapter the finite element model and different topology optimization results have been presented. Additionally, analysis of the material costs for cast parts was conducted. Results from presented analysis will be used as an input to propose mass reduced design of the nacelle components, which will fulfil design requirements for 10MW wind turbine.

2.3 Reduction of nacelle mass

2.3.1 New design of components

The optimization algorithm used in the study alters the material distribution to minimize mass of analysed components under given stiffness of the structure and within ultimate stress limits. The results of topology optimization are the values of design variable within assumed design area, in cases presented in the report it is density of finite elements. The next step of the study is to convert the topology optimization results into reasonable design models. The new design of the mass reduced components should be possible to manufacture by casting and fulfil design requirements. In the report two modified designs of the mainframe and king-pin are proposed. Two designs are proposed based on topology optimization results with displacement constraint of 15 mm and 20 mm. The optimization case with displacement constraint of 30 mm was neglected due to the high stress values close to yield point.

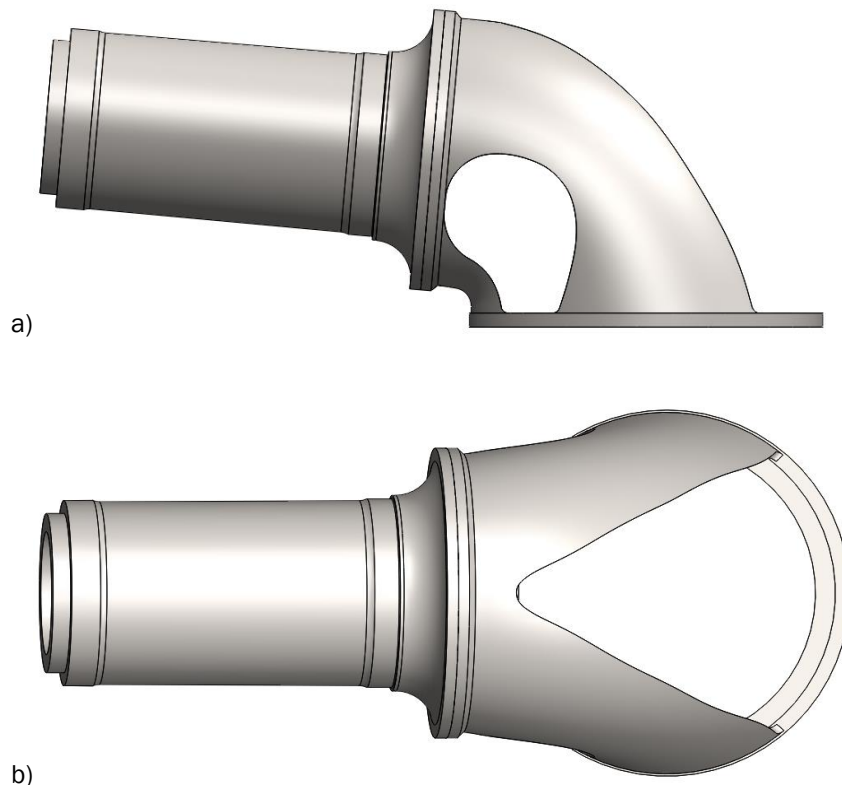


Figure 14 Modification of design for mainframe and king-pin – design 1, a) side view, b) top view

In Figure 14 the new design for the mainframe and king-pin is proposed, is based on the first optimization results, and in further part of the report will be called “design 1”. In this case material was removed from sides and bottom back part of the mainframe. In the side holes in component additional fillets were added to avoid high stress concentration areas. Additionally mass of the king-pin was reduced by decreasing thickness of the cylinder wall that connects the upwind and downwind bearing support by 10 mm.

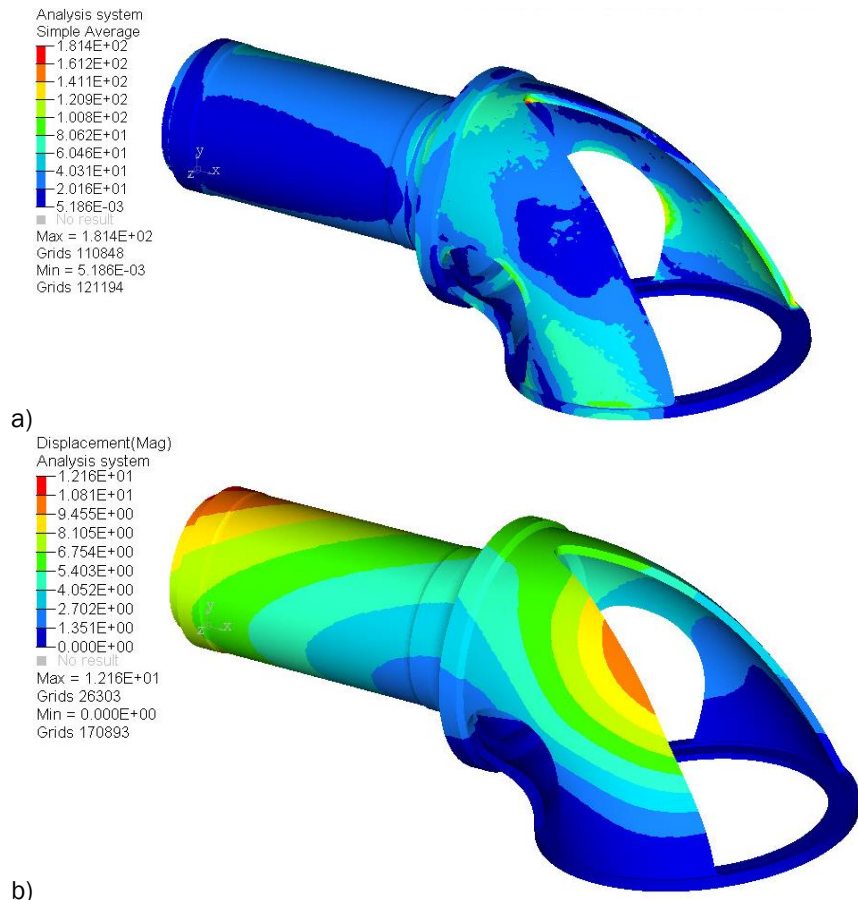
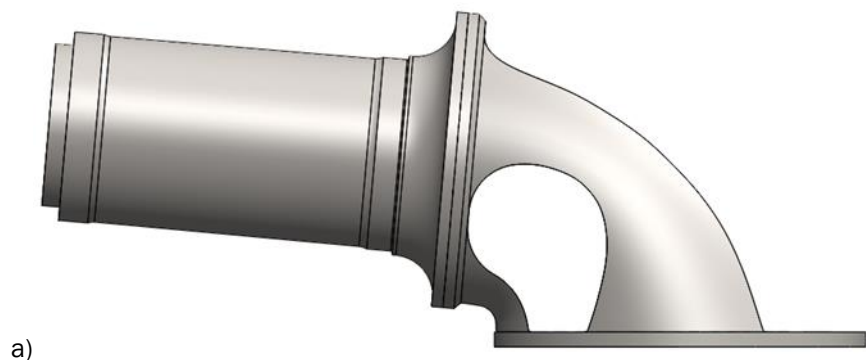
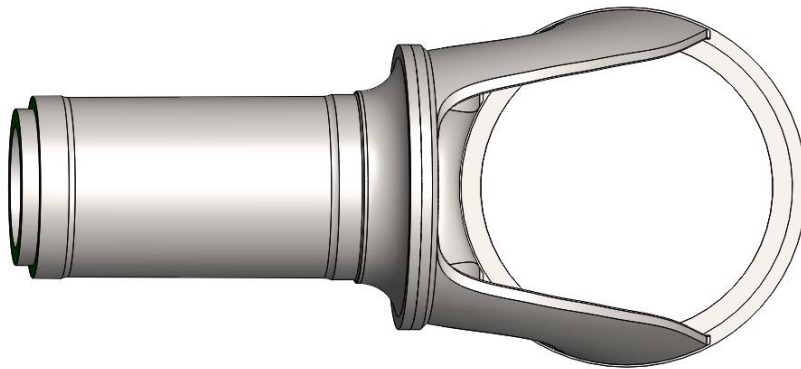


Figure 15 Ultimate design 1 finite element analysis,
a) von Mises stress [MPa],
b) displacement magnitude [mm]

The proposition of new design was verified on the basis of ultimate stress distribution and deformations under extreme loads. Applied loads in the simulation were described in chapter 2.2.1. Analysing simulation results presented in Figure 15 one can observe that von Mises stress reaches value of 181 MPa and the maximum stress concentration point is in the fillet around the removed material region. The stresses increases to about 100 MPa in comparison to the initial design, but they are under safety value which is 246 MPa. The deformation of the structure under applied loading is lower the set maximum in the optimization problem.





b)
Figure 16 *Modification of design for mainframe and king-pin – design 2,*
a) side view,
b) top view

The second lightweight design is based on the optimization results with displacement constraint of 20 mm, and will be called “design 2”. The CAD model of the design 2 is presented in Figure 16. In this case, the material was removed from sides of the mainframe in the same way like in the previous concept, and the back hole extended to remove material until flange connecting to the king-pin. Thickness of the king-pin wall between the upwind and downwind bearings support was reduced by 30 mm.

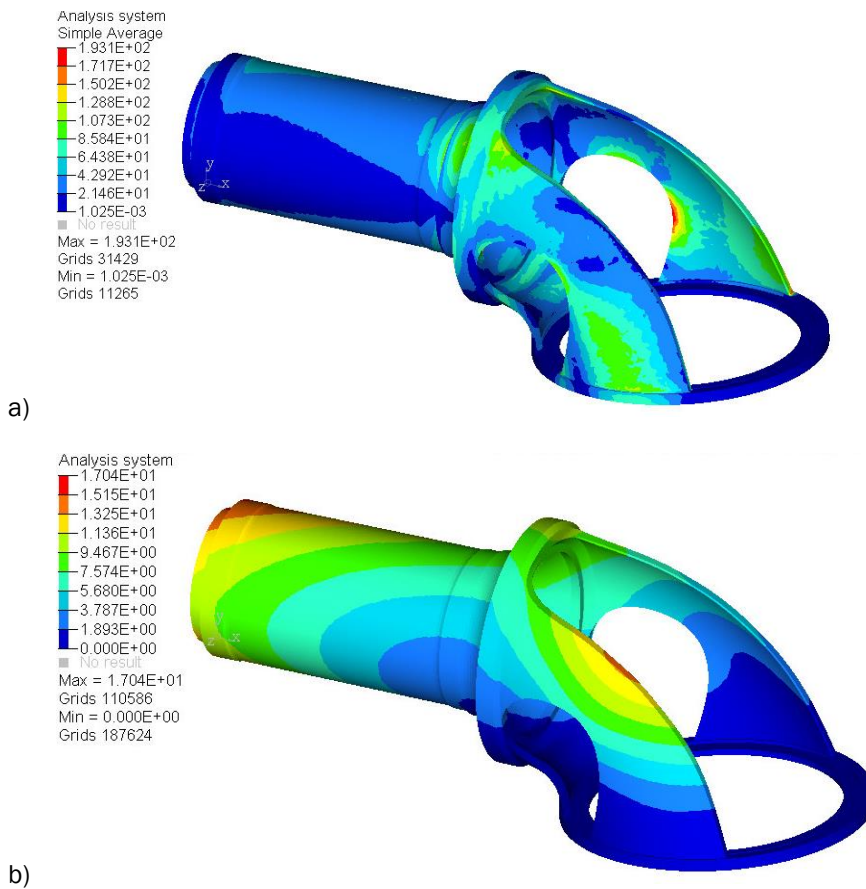


Figure 17 *Ultimate design 1 finite element analysis*
a) von Mises stress [MPa],
b) displacement magnitude [mm]

In Figure 17 the stress simulation results for new design are presented. The maximum value of stress in this case reaches 200 MPa and deformation up to 17 mm.

The two proposed designs are based on the topology optimization results and are characterized by significant mass reduction in the mainframe, but also higher ultimate stresses and deformation under the design loads. The modification of the mainframe by removing material from sides and back of component will influence bending stiffness of the structure and torsional stiffness. The changes of stiffness will change natural frequencies of the structure which should be analysed in the final design.

2.3.2 Comparison of proposed designs

To make a choice for the mass reduced design which will be characterized by maximum of reduced mass and proper mechanical properties, in this chapter comparison of proposed concepts is done. Firstly, maximum stresses in the structure and deformations under design loads were compared in order to verify safety of analysed structures. In table 3 the results of the finite element analysis for the new concepts are compared with the initial design.

Table 3. FE results comparison

Design	Max. von Mises stress	Max. displacement	Design stress limit	Weight of structure
Initial Design	87 MPa	6 mm	246 MPa	122,219 kg
Design 1	181 MPa	12 mm	246 MPa	99,281 kg
Design 2	193 MPa	17 mm	246 MPa	82,621 kg

On the basis of information in table 3, one may conclude that safety of the structure is retained; the stresses do not exceed the design value, as well as the deformation is lower than assumed value of 20 mm. As it was mentioned in previous chapter, mass reduction and modification of components geometry will influence torsional stiffness the king-pin and mainframe, which is important from point of view of a controller and generator. The torsional stiffness of analysed structure was estimated by applying only generator torque to the king-pin connected with mainframe which was constrained on the yaw bearing. In table 4 the torsional stiffness of analysed designs is presented.

Table 4. Torsional stiffness of analysed concepts

Design	Torsional stiffness
Initial Design	21.7e9 Nm/rad
Design 1	9.2e9 Nm/rad
Design 2	5.5e9 Nm/rad

The torsional stiffness for new designs decrease, for design 1 is about 57 % with comparison to the primary structure, but between design 1 and design 2 the difference in torsional stiffness is about 3.7 GNm/rad what is only 17 % of the primary design stiffness. Finally, the comparison of mass reduction for proposed geometries is presented hereunder

Table 5. Mass reduction summary

	Initial design	Design 1	Design 2
King-pin mass	57,043 kg	55,225 kg	49,927 kg
Mainframe mass	65,176 kg	44,056 kg	32,694 kg
Total mass	122,219 kg	99,281 kg	82,621 kg
King-pin mass reduction	-	3.2 %	12.5 %

Mainframe mass reduction	-	32.4 %	49.8 %
Total mass reduction	-	18.8 %	32.4 %

By reduction of the king-pin wall thickness in design 1, it was possible to reduce its mass by 3.2%, and by reducing it by 30 mm in the design 2 the element mass has decreased about 12.5 %. By changing geometry of the mainframe on the basis of topology optimization results mass of the component was decreased by 32.4 % in the first concept, and almost 50 % for the second one. Overall mass reduction for analysed structure that is the king-pin connected with mainframe is 18.8 % for the design 1 and 32.4 % for the design 2. Comparing both proposed concepts, design 2 is characterized by higher maximum stress level under design loads and lower torsional stiffness than design 1, but these differences are relatively small with possibilities of mass reduction which gives design 2. The second design allows for 13.6 % higher mass reduction of the structure than the first one, and it fulfil design safety requirements for these reasons it was chosen as the design concept for further analysis.

2.4 Bolted connection between components

2.4.1 Flange connection

Connection between the nacelle components is crucial because all loads derived from the rotor and generator are transferred by a drivetrain, mainframe and tower to the ground. To connect the nacelle structural elements mostly bolted joints are used. The bolted assembly consists of the bolt group (head, stud, and nut) and flanges (top and bottom) [16]. Because of different loading conditions and high loads acting on wind turbines, the bolted connections can separate or fail. To minimize failures, pretension is applied to the bolts, which insures that the connection will not separate and provided better fatigue resistance [16]. The model of bolted connection is presented in Figure 18.

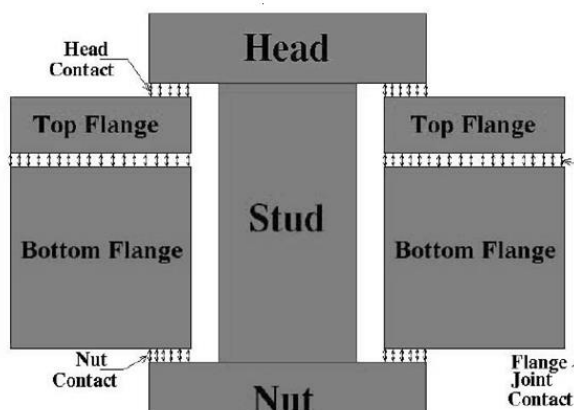


Figure 18 Model of bolted connection [16]

In the bolted connection, the surfaces of two flanges are in contact against each other, also contact surface exist between the head of bolt and the flange as well as the nut and the flange. Bolted joints can be modelled in different ways depending on complexity of the model. In the study solid bolt model has been used [16]. Such model is the most realistic representation to simulate bolt because it can captures bending, tensile and thermal loads. This approach also allow for full stress distribution in head, nut and stud. The disadvantages of this method is complex solid element model which contains contact elements, this will increase model preparation time and computational time.

In the report, two connections methods between the mainframe and king-pin were investigated. The first one assumes that two components are connected by flanges with one bolt row, and in the

second one the mainframe and king-pin are connected by two rows of bolts which are located in opposite directions. Bolts strength and mechanical properties are standardized according to ISO 898/1-2 [17]. In the study, connection bolts with nominal size M48 and class 10.9 according to ISO 4014 are initially used, for which heavy duty flat washers were selected according to DIN 6340. The class of the bolt is characterized by two numbers separated by a dot. The first number is 1/100 of the minimum ultimate strength measured in MPa, and the product of the two numbers is 1/10 of the minimum yield strength, also measured in MPa [17]. The chosen bolt here is 10.9 what means that it has a minimum ultimate strength of $100 \cdot 10 = 1000$ MPa and a minimum yield strength of $10 \cdot 10 \cdot 9 = 900$ MPa. In this analysis, the most common bolts without surface treatment, which are called black bolts, are used [17]. The number of bolts in flanged connection is limited by bolts size. The distance between bolts usually should be higher than three times the bolthole diameter [18]. In the connection between the mainframe and king-pin 60 bolts were assumed and the flange was designed, what is presented in Figure 19.

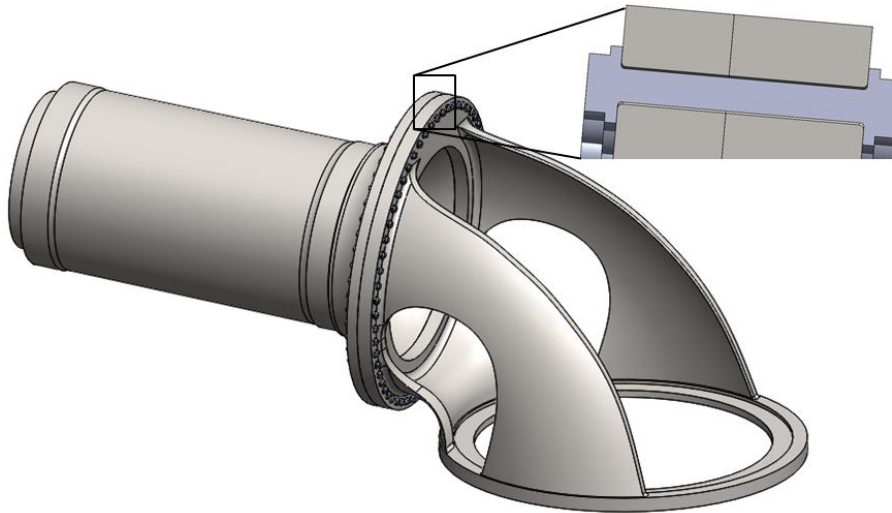


Figure 19 Mass reduced design of king-pin and mainframe connected by flange

For designing bolted connections, it is important to determine the appropriate preload for the bolts. A basic method for this is to use 70 - 80% of the proof strength [17], which is used mostly for removable fasteners. Applying preload on bolts the tension in bolts and contact stresses between head of bolt and flange should be considered either. From point of view of the fatigue strength higher pretension is preferable. Equation (1) represents the formula to calculate pretension force on a bolt.

$$F_{pret} = A \cdot G_f \cdot \sigma_y \quad (1)$$

where $A = 0.0018 \text{ m}^2$ is the bolt cross section area, G_f is the pretension factor equal to 0.7 and $\sigma_y = 900 \text{ MPa}$ yield strength of the bolt. The pretension force calculated from equation (1) is 798 kN

In this study, a finite element approach was used to verify the safety of the bolted joint, where a linear analysis was used to simulate stresses in the connections. It allows for accurate representation of geometry and loading effects in bolts as well as limited contact effect [16]. Contact elements were used between the bolt heads and top flange and the bolt nuts and bottom flange, between flanges contact elements with friction were modelled. Pretension force was applied to each bolt using 3D contact surface predefined in the centre of studs. Applied pretension force in the finite element simulation was 700 kN Distribution of stresses in the king-pin and mainframe connected by bolted flange is presented in Figure 20.

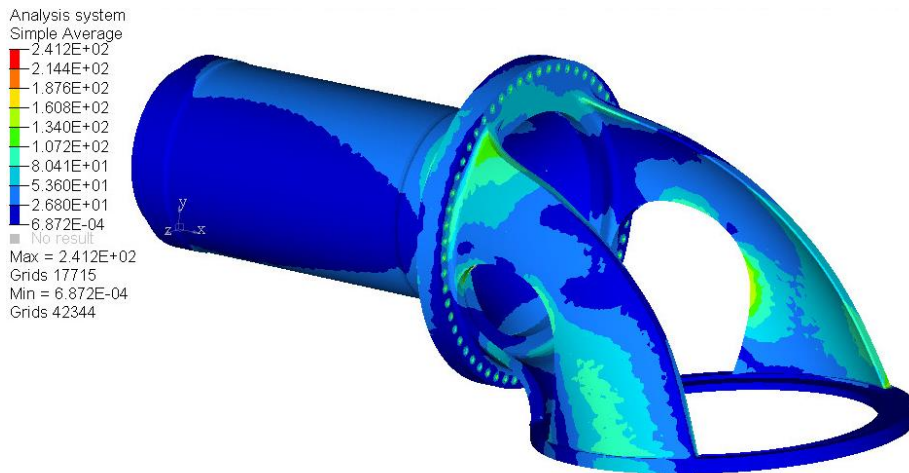


Figure 20 Stress analyses in bolted flange connection and components

The analysis presented above was conducted for wind turbine components under operational loads that were defined in chapter 3.1, and preloaded bolted connection. In the structural components with bolted joints the main stress concentration points are due to contact stress between the head and nut of bolts and flanges. In the analysed design, the maximum stress reaches 241 MPa in the flange, also it is visible that in the mainframe there is no low stress concentration areas in comparison to results presented in figure 4, which means that structure with reduced mass works optimally. In Figure 21 the stress analyses in flange and bolt is presented.

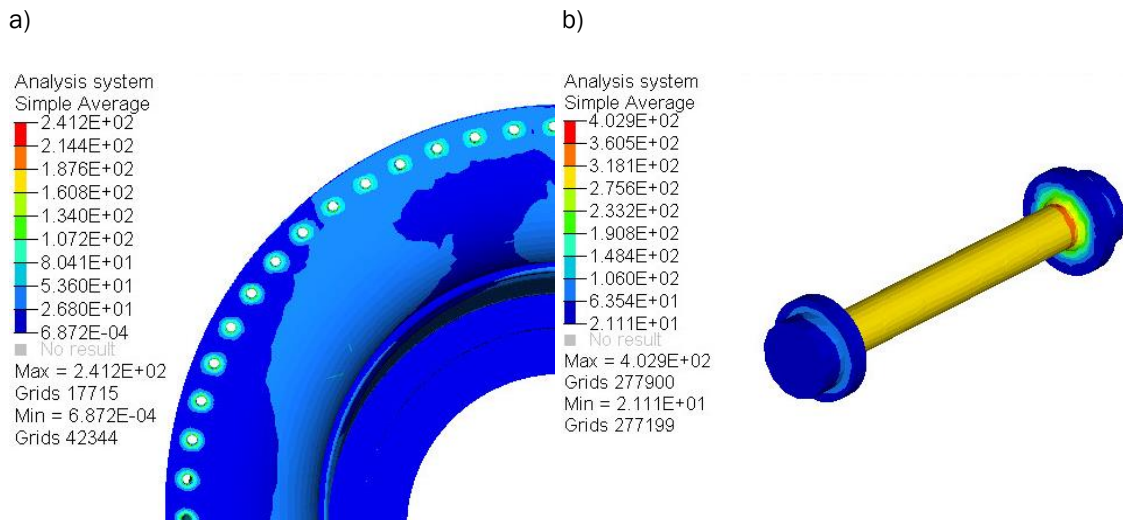


Figure 21 Stress analyses in flange and bolt, a) front flange view, b) stress in bolts

In case of the bolted flange connection, the highest stresses are in the flanges and they are higher than stresses without the bolted joint, which was analysed in chapter 4.1, and the difference between both cases is about 48 MPa. The level of stress in structure with bolted joint mostly depends on the pretension force which is applied to bolts. Analysing results in Figure 21 b one can see that stresses in bolts are concentrated in the fillet between the stud and head, and it is the point that can fail with the most probability.

2.4.2 Two stud connection

The mainframe and king-pin can also be connected by bolts which are directly connected to the opposite flanges by threads, as two rows of bolts. For this connection, bolts with nominal size M36 and class 10.9 according to ISO 4014 were used with heavy duty flat washers (DIN 6340). The pretension force was calculated from equation (1), for chosen bolts it is 641 kN. In the joint due to dimensions between bolts and its size 60 bolts was assumed.

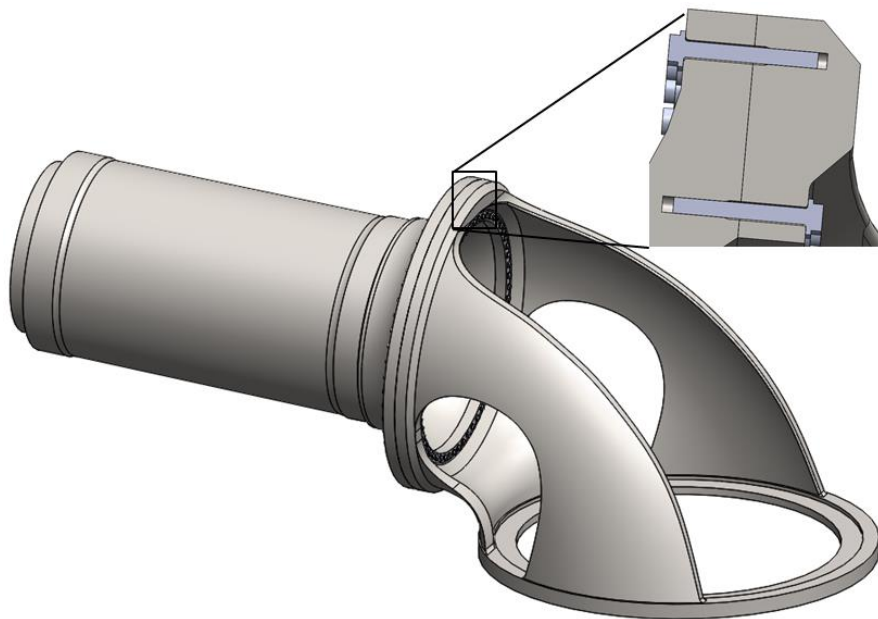


Figure 22 Mass reduced design of king-pin and mainframe connected by two parallel bolts

In Figure 22, CAD model of the king-pin and mainframe and joint with double row bolt is presented. In this case the fasteners pressing equally flanges from bottom and top. The flanges do not have to be modified regarding to the initial design. The stress analysis results for this connection are presented in Figure 23.

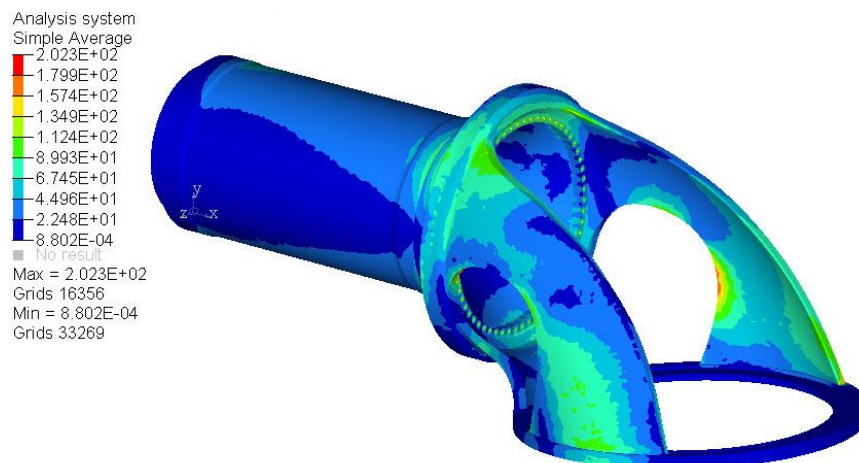


Figure 23 Stress analyses in bolted flange connection and components

The applied preload in this model of joint is 500 kN, and the stress between bolts and flanges decreases as compared to the previous example. In Figure 24 view on detailed results in conducted analysis are shown.

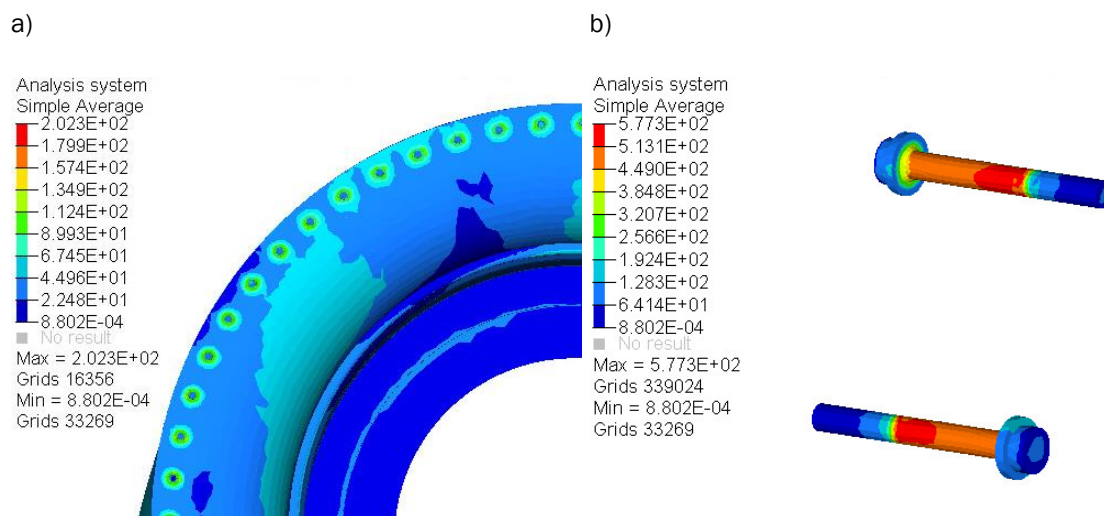


Figure 24 Stress analyses in flange and bolt, a) front flange view, b) stress in bolts

The stresses in the bolted components are larger by 10 MPa compared to the primary design (figure 4). Distribution of stress in fasteners is different than in the model presented in previous chapter, it is because of threaded connection between stud and flange.

The safety of bolted connection in both analysed cases was verified by 3D finite element simulations. The yield strength of bolts class 10.9 is 900 MPa which gives design level of 643 MPa with assumed material safety factor of 1.4. The maximum value of von Mises stress in the model presented in Figure 21 b is 403 MPa, and the model presented in Figure 24 b gives level of 577 MPa and in both cases the maximum stresses are lower than the design value for chosen class of bolts. Comparing stress distribution between two used fasteners, in the first case loading is distributed equally in the stud and the stresses are concentrated in the fillet between stud and head, but in the second example maximum level of stress appear in the thread. In the finite element model, the thread was modelled by connecting elements on the thread surface between the stud and flange, which is a simplification of the thread connection and can introduce additional uncertainty in the results. Comparing the two connection methods between the king-pin and mainframe, one can observe that the application of two rows of bolts in opposite sides will provide uniform compression force to flanges, and lower stress level on structural components. Also this method of connection will give higher safety because of application of two rows of fasteners.

2.5 Mass reduced tower top concept

Beside of the analysis presented in previous chapter, the bolts strength depends also on the geometry of connected parts which determines uniform transfer of loads in the flanges. A low local stiffness at the flange might lead to undesired deformations and these deformations will lead to a decrease of the bolts strength [12]. In topology optimization presented so far in this report, the bolted connections between the king-pin and mainframe as well as yaw bearing were not taken into account. The new design of mainframe proposed in the study is herein corrected due to structural stiffness in these areas. Additional topology optimization case was conducted to get a view on the mass distribution in case of maximum rigidity of the structure. In this analysis stiffness of the king-pin and mainframe was assumed close to the primary design (5 mm higher displacement of nodes on upwind side of king-pin with comparison to primary design). Applied loads included the torsional moment, rotor bending moment, thrust force and side rotor moment. The results from this optimization case are presented in figure 25.

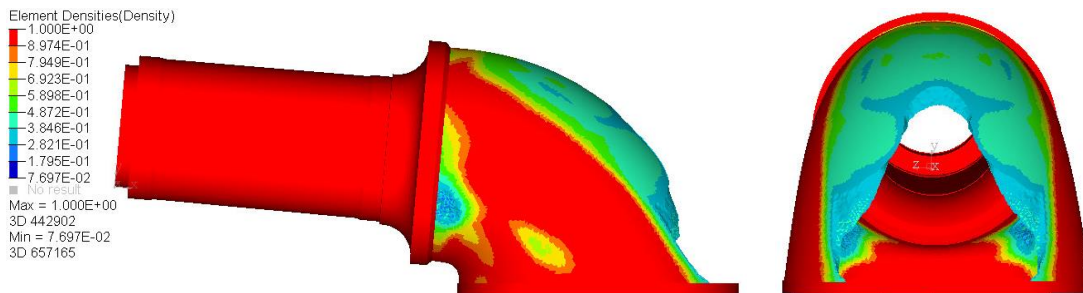
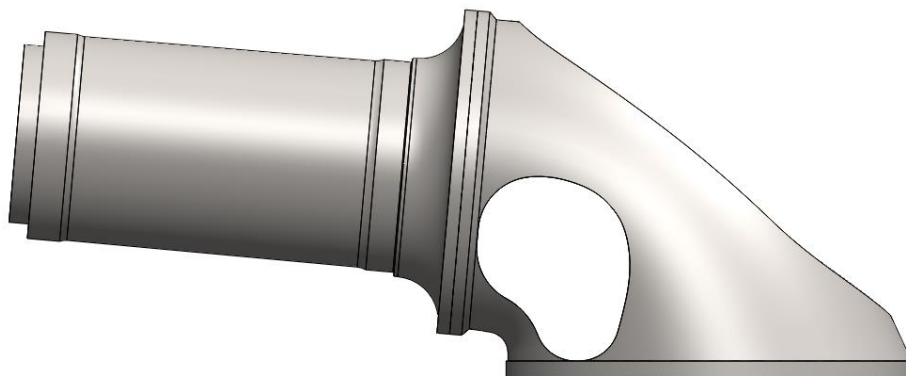


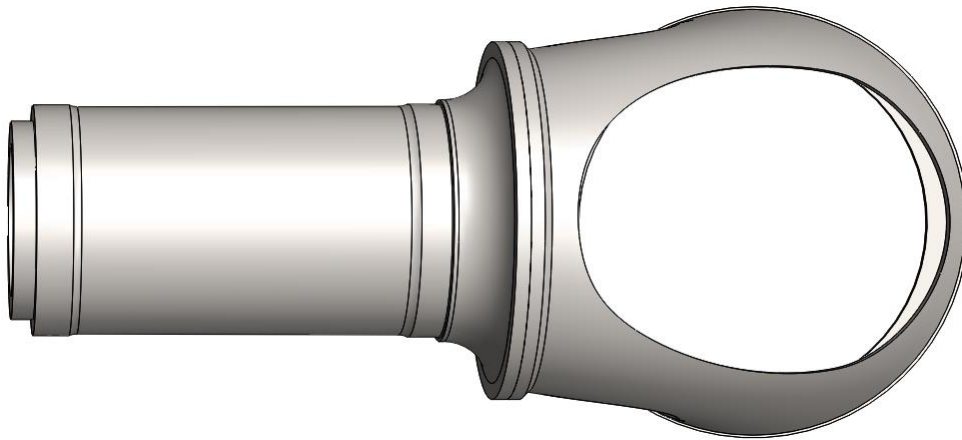
Figure 25 Topology optimization results for displacement constraint 5 mm and element density more than 0.3

In the optimal design, the mass was reduced in the back side, where material has been removed in the bottom side of the mainframe and element density reduced in the upper side. This suggests that to increase stiffness of the prior obtained design 2, it is necessary to add material in the upper and lower side of the back cut in the mainframe.

In the analysed model, yaw bearing was not considered and the constraint fixing all 6 DOFs of the nodes in its area was modelled. This assumption may provide unrealistic behaviour of the model in the yaw connection, which in conducted optimization leads to the topology which will not distribute loads uniformly on the yaw bearing. To avoid stress concentration areas and low local stiffness in this area as well as in the flange connection to the king-pin proposed design was modified by adding fillets in made holes. In figure 26, geometry of the king-pin and mainframe after corrections is presented.



a)



b)
Figure 26 Geometry of king-pin and mainframe after correction of topology,
 a) side view,
 b) top view

To verify the safety of proposed design and rigidity of the structure finite element analysis was conducted. In the analysis torsional moment from generator (16,500 kNm), rotor bending moment (16,500 kNm), thrust force (4,600 kN) and side rotor moment (10,000 kNm) were applied as described in chapter 3.1. The results of FEM analysis are presented in figure 27.

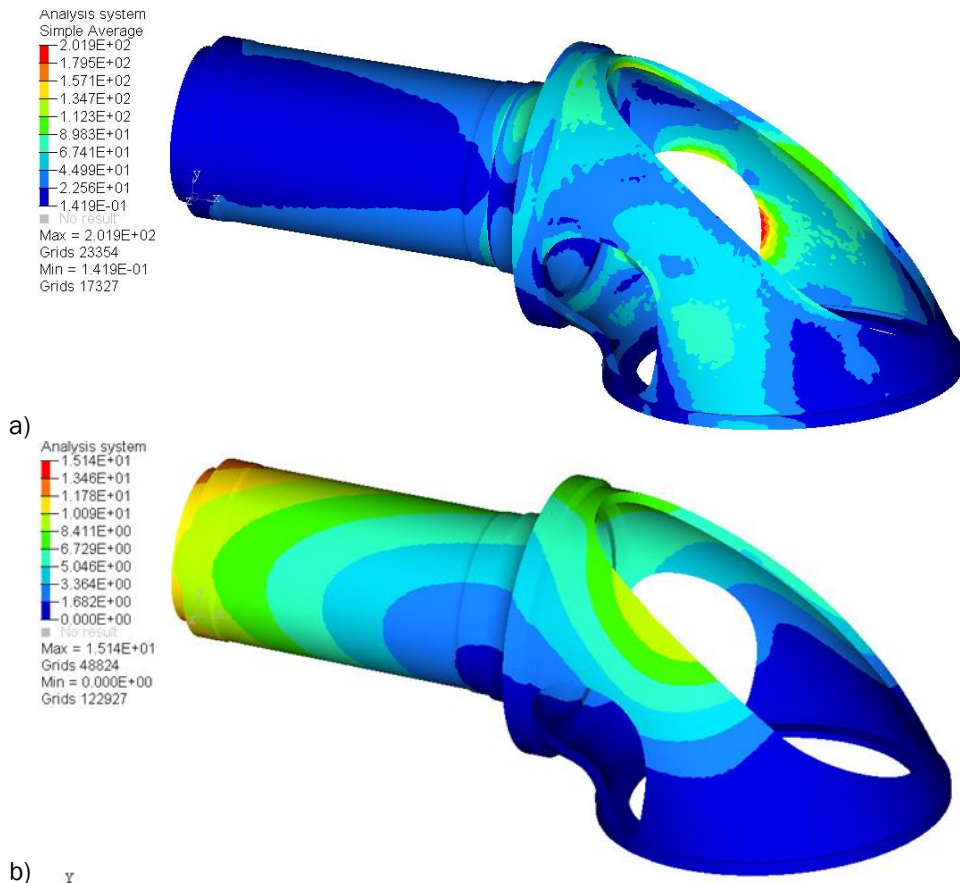


Figure 27 *Ultimate design 1 finite element analysis,*
a) von Mises stress [MPa],
b) displacement magnitude [mm]

Proposed new design fulfils safety requirements, maximum von mises stress with level of 201 MPa are lower than design level of 246 MPa, and the deformation of the structure do not exceed 15 mm.

Modifications of the design beside of stiffening of the mainframe will increase its mass. The comparison of mass between initial design and final design is presented in table 6.

Table 6. *Mass reduction summary for final design*

	Initial design	Final design
King-pin mass	57,043 kg	49,927 kg
Mainframe mass	65,176 kg	43,084 kg
Total mass	122,219 kg	93,011 kg
King-pin mass reduction	-	12.5 %
Mainframe mass reduction	-	33.9 %
Total mass reduction	-	23.9 %

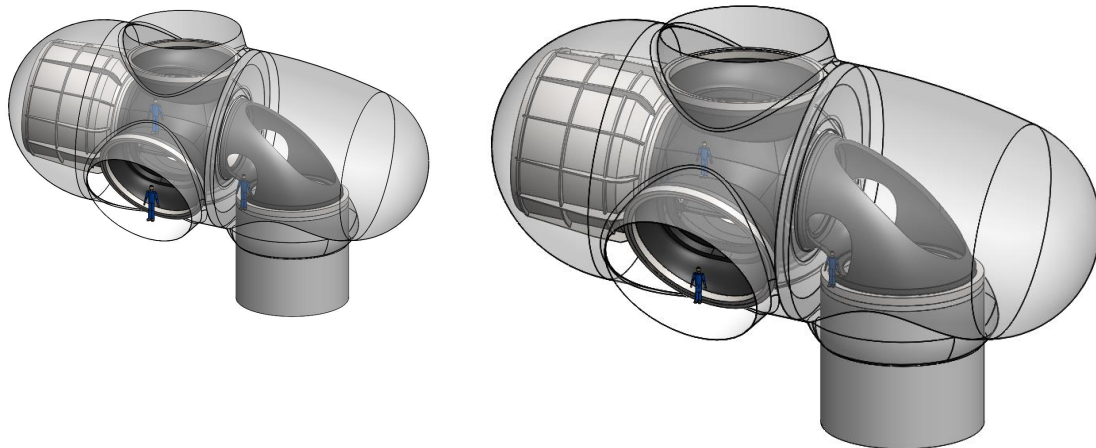
After stiffening of the mainframe by adding additional fillets its mass increase about 15 %, with comparison to the design 2. As a result of analysis conducted in the report total mass reduction of the nacelle components for 10 MW wind turbine was 24 %.

With comparison to the 10 MW baseline turbine the mass of the nacelle (minus generator and main bearing) was reduced about 17 %. The corresponding Capital expenditure (CAPEX) for the baseline turbine is 486,000 €, for the initial design of the king-pin 10 MW concept, it is 534,000 €. By reducing the mass in this study the new design has a Capex of 402,000 €. The LCOE estimation for the 10 MW baseline turbine is 93.5 €/MWh, initial design of king-pin turbine is 93.7 €/MWh, and for the mass reduced design is 93.2 €/MWh.

In terms of LCOE there is not much difference between baseline and proposed mass reduced concept for fixed base offshore wind turbines, it is only of the order of 0.23 %, but the difference in the top tower mass will have better impact on LCOE calculated for floating wind turbines. In case of a floating wind turbine the overall floater mass is related to the overturning moment from the tower top mass and thrust. Assuming the total moment arm from the tower top is a constant of from the hub height, the reduction in nacelle mass achieves a 1% reduction in overturning moment, which may translate to a maximum 1% saving in floater Capex and an overall saving in LCOE of about 0.5%.

2.6 Concept of a 20 MW Turbine

The upscaling rules were used to present design concept of 20 MW wind turbine. According to Sieros [19] if geometrical similarity is enforced, the weight and power in a wind turbine scale according to $m \sim s^3$ and $P \sim s^2$ where s is the scaling factor. The mass reduced design of 10 MW wind turbine was upscale to 20 MW, and presented in figure 28.



a) b)
Figure 28 Schematic of direct-drive wind turbine,
 a) 10 MW turbine,
 b) 20 MW turbine

A feature of the 10 MW turbine is a large blade root diameter, about 5.4 m, which after up scaling will correspond to diameter of 7.6 m for 20 MW turbine. Such diameter of blade root can cause difficulties in the pitch mechanism especially in the design of such a large pitch bearing. In this study, structural redesign of the blade for the 10 MW turbine was also done so that a reduced root diameter is obtained, which can be applied after upscaling to 20 MW wind turbine.

The outer geometry of the blade was modified in the region between the root ($r = 2.8$ m) and maximum chord, which is approximately at $r = 24$ m, the analyses allowed to reduce root diameter to 4.6 m, and were performed on the basis of [5]. In the study, only the chord distribution was modified as shown in figure 29. Relative thickness and twist were left unchanged.

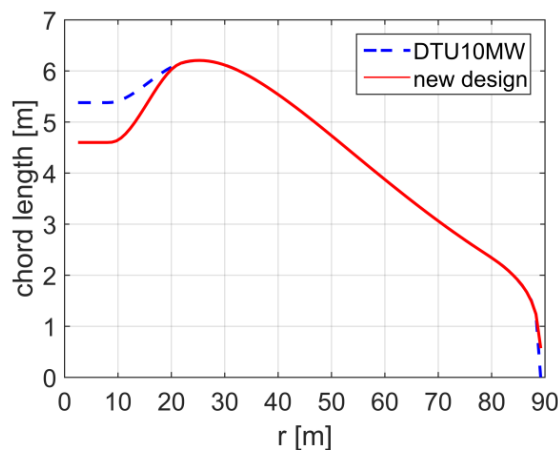


Figure 29 Chord distribution

The composite layup in the root region was changed increasing the total thickness of the composite materials by up to 19 %. This leads to a mass per length distribution very similar to the original design. The composite layup remained unchanged for $r > 24.4$ m. In the new design small changes in flapwise bending stiffness and torsional stiffness in the region between $r = 40$ m and $r = 60$ m were recorded with comparison to primary design, it is due to the small differences in the airfoil thickness.

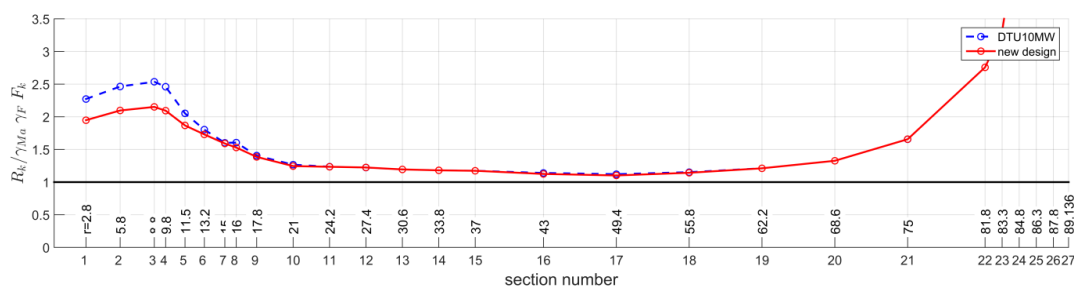


Figure 30 Strength analysis (minimum value of the left hand side of Equation (4.19) from [5] found at each section)

Strength analysis was performed using the same methods and loads as described in [5]. The results are shown in figure 30. The design is safe as all values in figure are larger than 1.0.

Reduction of the blade root diameter allowed decreasing the oversized blade diameter in the root region with fulfilment of the safety requirements. The redesign of the blade does not influence its mass, but smaller root diameter will allow decreasing the mass of the hub, e.g. bolted connection between blade and hub and pitching mechanism, which will be important for 20 MW wind turbine.

2.7 Conclusions

In the report, an optimal reduced mass nacelle design of the innovative 10 MW offshore reference wind turbine was presented. In this study it was shown that ultimate stresses on the nacelle components did not exceed the design limit and several areas on the components had low stress concentration, providing the means for mass reduction. Presented analysis shows that structural mass of the nacelle components can be reduced without significant influence on the mechanical properties of the structure, e.g. for the mainframe the mass can be reduced from upper and side parts, and for the king-pin wall thickness can be decreased. The topology optimization methods were used to propose new design of the wind turbine components, and the nacelle configuration that provides minimum cost for large capacity offshore wind turbines.

The two lightweight designs for the king-pin and mainframe were proposed, the first one allows for mass reduction about 19 % and the second one by 32 %. The torsional stiffness of the king-pin for mass reduced topologies decreases for the new geometries about 57 % and 73 %, but the resulting displacement of the structure are still constrained to the set limits. Comparing the two proposed concepts, the design 2 is characterized by higher ultimate stresses under extreme loads and lower torsional stiffness than design 1, but these differences between both proposed solutions are relatively small. The design 1 provides 13.6 % higher mass reduction than the first one, so it was chosen as the concept for the final topology. In topology optimization yaw bearing and bolted connection between the king-pin and mainframe were not taken into account, what can leads to uniform transfer of loads in this areas and low local stiffness, what can result in failures during operation. To avoid of such behaviour of the structural components proposed design was modified by adding fillets stiffening the structure. After correction of the mainframe topology its mass increases about 15 %, with comparison to the design 2. Finally, the total mass reduction of the nacelle for direct-drive 10 MW wind turbine was obtained 24 % with respect to the initial design.

The two joint concepts between the king-pin and mainframe were analysed: bolted flange and two row bolts. Application of two rows fasteners will provide uniform compression force to flanges and lower stress level on the structural components, what provide higher safety than bolted flange connection. The safety of the final design and joint were verified by finite element simulations. Additionally, in the report reduction of the blade root diameter was presented, which allowed to

decreasing the oversized blade diameter in the root region. The redesign of the blade will allow decreasing mass of the hub e.g. bolted connection between blade and hub, and reducing size of pitch mechanism what will be important for 20 MW wind turbine case.

Material and manufacturing cost estimated by CAPEX shows 17.3 % reduction for new king-pin design with comparison to the 10 MW baseline turbine. In the terms of LCOE, there is a 0.5% reduction in the case of 10 MW floating wind turbines, but there is hardly any reduction for fixed base offshore wind turbines.

Limitations of proposed design are its susceptibility to bending and torsional loads caused by the removal of the material in back side of the mainframe, in view of this in topology optimization additional load cases should be considered like side loads acting on the nacelle. The structure that allows increasing to stiffening the mainframe can be added e.g. ribs connecting side walls of the component. In the future work geometry of mass reduced design can be improved to avoid stress concentration areas which occur in the side holes of the mainframe, and influence of the geometry modifications on natural frequencies of the structure will be studied. Mass reduction of a wind turbine load carrying components will influence their stiffness which is important from the point of view of resonances in a turbine. The bending stiffness of a mainframe will influence its modes which can be close to the tower natural frequencies for this reason the modal analysis of this component has to be conducted. In presented report the generator weight was neglected but it also will have influence on extreme loads, in the future study the influence of generator on dynamics can be considered e.g. by development of a proper model in an aero-elastic code which also allows more accurate determination loads in 10 MW direct-drive turbine. The yaw bearing and tower deformations under operational loads should be included in the model as well to avoid failures in yaw mechanism.

3 VARIABLE AXIAL INDUCTION DISTRIBUTION ALONG THE ROTOR SPAN

3.1 Concept description

The general concept that is being investigated in this section is to determine the influence on the LCoE of induction variations along the span of the rotor blade. In previous studies it has been investigated what the influence can be of a lower axial Induction factor for the complete rotor.

The concept is being investigated by changing the axial induction factor along the span due to changes in chord distributions along the span. The following chord distributions are analysed:

1. The reference blade
2. Constant relative reductions along the span of x%
3. Blade root reduction of x% with a linear decrease of the reduction to 0 at the tip
4. Tip chord reduction of x% with a linear decrease of the reduction to 0 at the blade root.
5. Linear increase of the chord along the span.
6. Root chord increase linear decreasing to the reference tip chord.
7. Tip chord increase linearly decreasing to the blade root chord.

The chord decreases that have been analysed are 10% and 20%. The resulting chord distributions are shown in the [Figure 31](#) and [Figure 32](#)

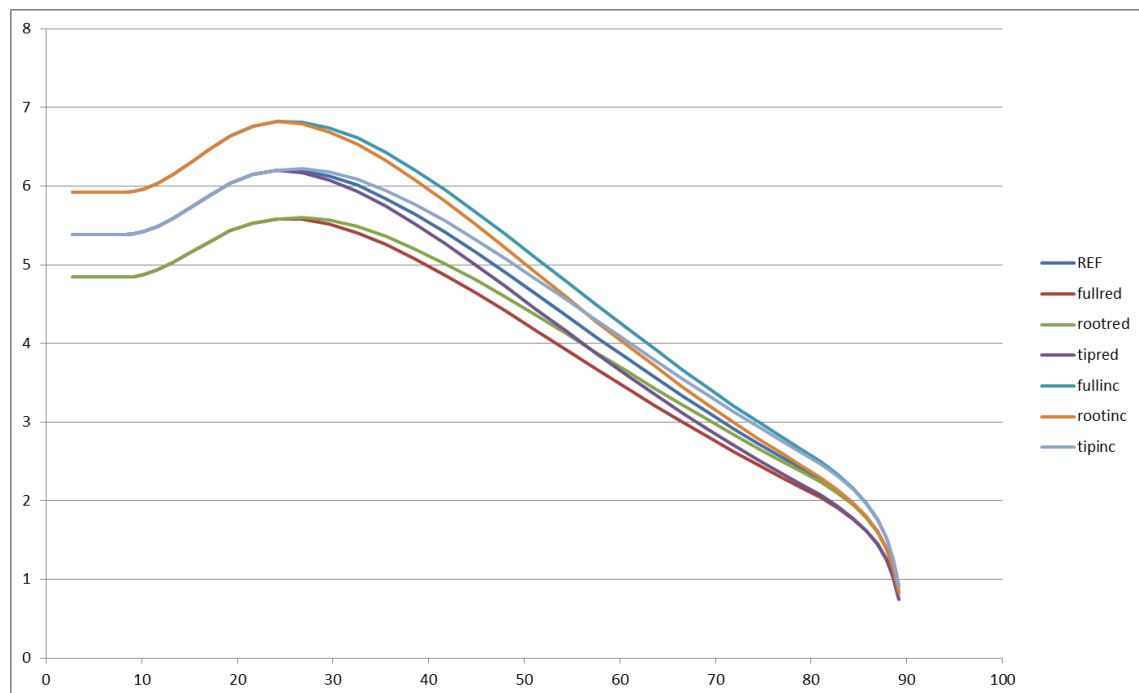


Figure 31 The chord distributions with a 10% variation

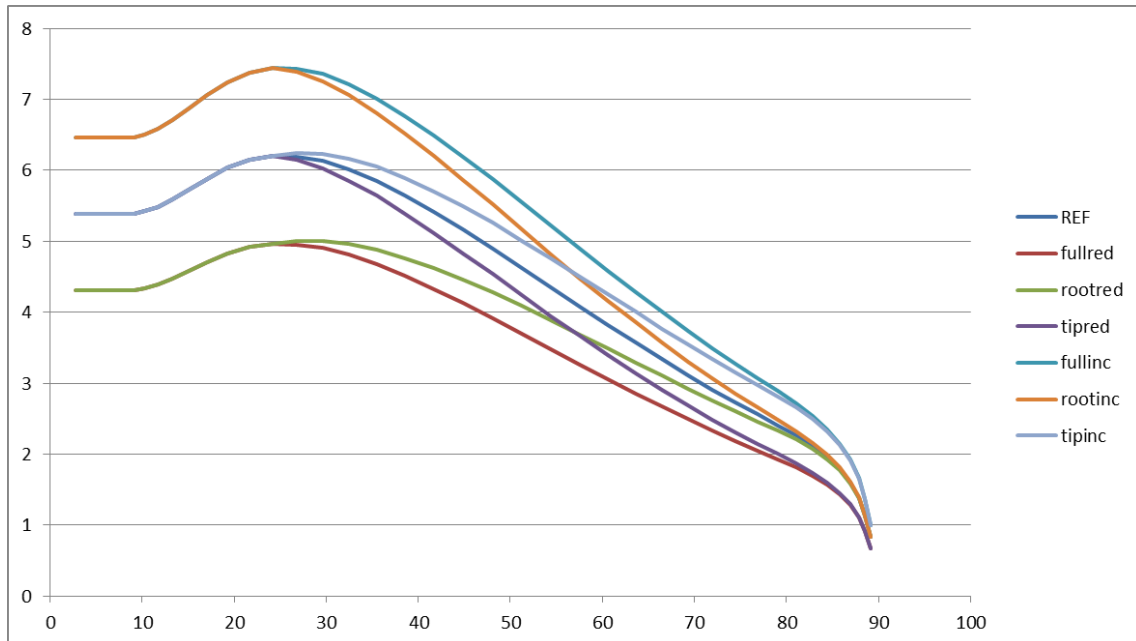


Figure 32 The chord distributions with a 20% variation

To determine the influence of the design variations an analysis has been made with the ECN tool BOT [20], to determine the axial induction along the span. The results are shown in figures below.

3.2 Cost Model

The cost model applied is the INNWIND.EU cost model developed in task 1.2 where it is assumed that the innovations investigated will only have effects on the Energy Yield, the cost of the blades and the cost of the tower. In reality there will also be an effect due to the difference C_T due to the fact that this will influence the wake effects and the overall wind farm efficiency. A lower C_T will result in higher wind farm efficiency and a higher C_T will reduce the wind farm efficiency.

The Energy Yield will be evaluated on the basis of the power curve that is calculated for each different distribution of the axial induction. The wind speed distribution used to evaluate the effect on the annual energy yield is a Weibull distribution with a shape factor K of 1.7 and an average wind speed of 7 m/s at 10 m height. This extrapolates to an average wind speed of 10 m/s and a Weibull shape factor of 2 at the hub height.

Due to the fact that engineering cost models usually underestimate the cost of the components the only the relative influences are used, i.e, the yield and the cost of rotor blades and tower are all taken relative to the result for the reference design given in [5] and the excel file with the aero-elastic description of the INNWIND.EU reference machine.

The blade cost model and the tower cost model are describe in more detail in the following sections.

The results, the different yields, tower weights and blade weights are fed into the INNWIND.EU cost model to determine the influence on the Levelised Cost of Energy (LCoE).

3.2.1 The blade cost model

The price of the blade is determined by the weight of the blade in a simple manner:

$$Price = C_{blade} * \#_{blades} * Mass_{blade}$$

The C_{blade} is as given in the INN WIND.EU cost model \$ 1,09 * 13,084/kg = \$ 14,26/kg or € 1,09/1.32 * 13,084/kg = € 10,80 / kg

$\#_{blades}$ the number of blades of the wind turbine, in this case 3.

The $Mass_{blade}$ is the mass of the rotor blade of the composite parts.

The Mass of a rotor blade is calculated with a simplified rotor blade design model that makes use of simple slender beam theory. The loading on the blade is determined on the basis of a simplified load model that use the IEC load conditions, class 1 A, as input.

The blade is divided into three sections, the flange, the root and airfoil sections, see Figure 33. The flange cross section is cylindrical the profile cross section is created by an elliptical beam cross section that carries the load and thin sections in the shape of the aerodynamic profile.

The root section is where the cylindrical load carrying section transforms into an ellipse.

The elliptical beam section consist of two elliptical shapes the outer contour and an elliptical inner contour. By subtracting the inner contour from the outer contour a thin walled beam remains. The outer dimensions of this beam are determined by the chord and profile thickness. The height of the beam is assumed to be 95% of the profile thickness and the width of the beam is assumed to be a certain percentage of the chord. This percentage can be varied along the span in a linear trend. This beam is designed at each element section for fatigue and static strength. The entire

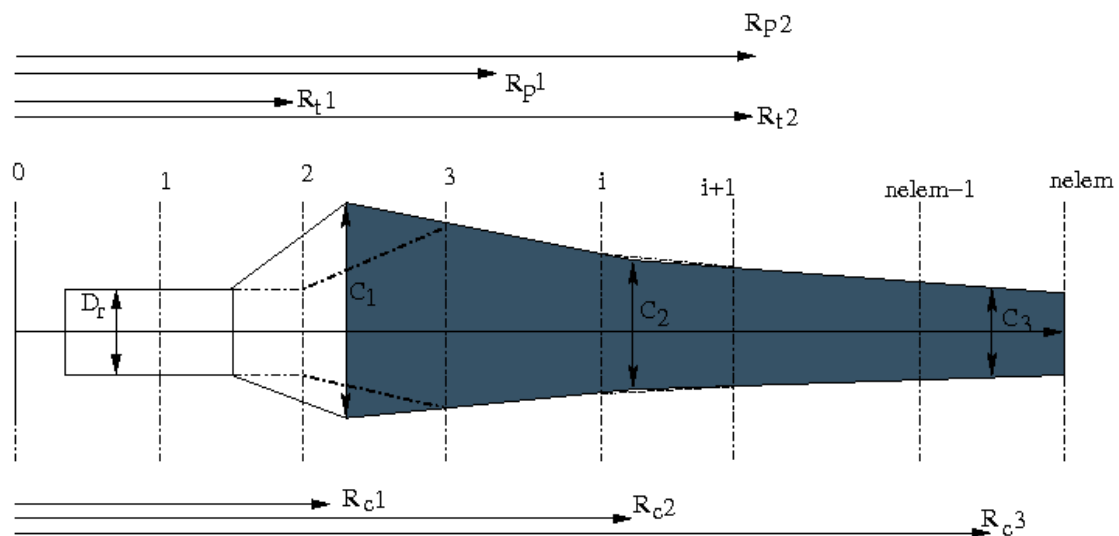


Figure 33 The blade model

beam is design to meet Eigen frequency and stiffness requirements.

The load spectrum for the rotor blade is also calculated in a simplified manner. The load spectrum is determined for 64 deterministic gusts that are based on the wind conditions defined in the input of the analysis. The wind spectrum can, and is in this case, based on the IEC wind conditions, IEC Class I A, ie. for an average wind speed of 10 m/s at hub height and the high turbulence¹ class.

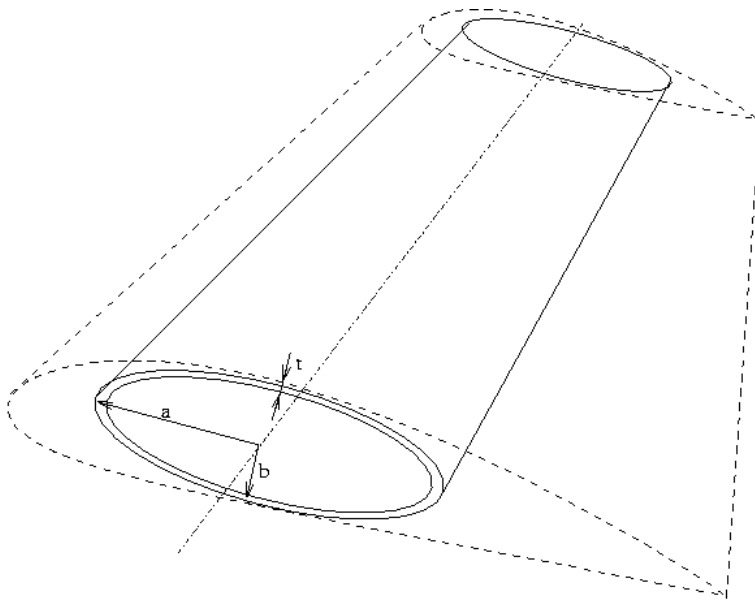


Figure 34 Airfoil section with a load carrying beam.

The load spectrum is determined without initially modelling dynamics for the blade. The mass and stiffness are initially not known. On the basis of the flapwise and leadwise (aerodynamic) loads on the tip the wall thickness of the tip element is determined and in the design loop the weight component in the leadwise load direction is added. At the end of the initial design loop, when all blade elements from tip to flange have been designed the mass and stiffness distribution of the blade is known and the Eigen frequency of the rotor can be calculated. With this and the rotor RPM versus wind speed the dynamic amplification factor for the stationary loads can be determined, increasing the loads and design loop is made once again changing the mass/stiffness distribution. This design loop is repeated until the outcome does not change anymore. This design loop results in a “final” mass and stiffness distribution of the blades. The mass of the blades is used in the cost model to determine the influence on the LCoE.

Due to the fact that the cost model is an approximation and due the fact that, especially engineering cost models usually under estimate the prices

3.2.2 The tower cost model

The tower cost is determined on the basis of the tower mass in a simple manner:

$$\text{Price} = c_{c_1} * \text{Mass}_{\text{tower}}$$

The value of c_{c_1} is $1,74 * \$ 2,5/\text{kg} = 1,74/1,32 * 2,5 = € 3,3 / \text{kg}$.

¹ Some discussion whether the high turbulence assumption is too conservative for offshore locations.

The tower weight is determined with a tower design model, which is based on a relative simple engineering model. This means that the tower dimensions, tower radius and wall thickness distribution is determined in such a way that the mass of the tower is minimal with the following design restrictions:

three strength requirements:

- 1 extreme loads,
- 2 fatigue loads,
- 3 buckling.

The tower design varies the taper of the diameter and the wall thickness linearly with the height.

Assumptions in the design model are that:

- ✓ $D_{iatop} = 1. + c_Dia_top * Dia,$
- ✓ $T_towerTop = 0.02 [m],$
- ✓ diameter varies linearly with the height,
- ✓ wall thickness varies linearly with the height.

In Figure 35 the model of the tower is shown.

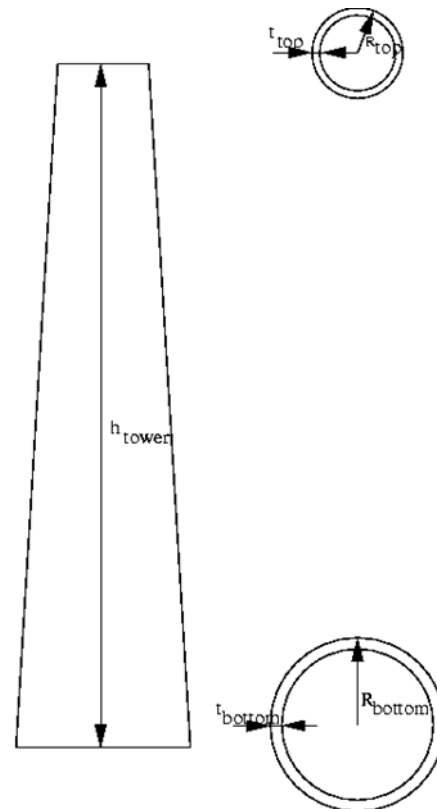


Figure 35 the tower model

Tower resonance requirements are shown in the table below:

soft-soft	v_{tower}	<	$a \cdot \Omega_{min}$		
stiff-soft	v_{tower}	>	$b \cdot \Omega_{max}$	&	$v_{tower} < a \cdot \#_blades \cdot \Omega_{min}$
stiff-stiff	v_{tower}	>	$c \cdot \#_blades \cdot \Omega_{max}$		

The strength and eigenfrequency of the tower is determined with simple beam theory, including the nacelle and rotor mass for the first bending eigenfrequency.

The model results in a simple tower design described with the tower taper and the wall thickness taper which together with the tower height and the top diameter gives a complete description of the tower. The resulting design complies with the given constraint w.r.t. eigenfrequency and has sufficient strength w.r.t. the given material strength parameters.

The engineering model results in:

- ✓ Mass_{tower}
- ✓ V_{tower}
- ✓ Tower foot diameter
- ✓ Tower footwall thickness.

3.3 Results

The different designs have been analysed with the BOT tool [20] tool. The different in axial distribution is shown in the Figure 36 and Figure 37

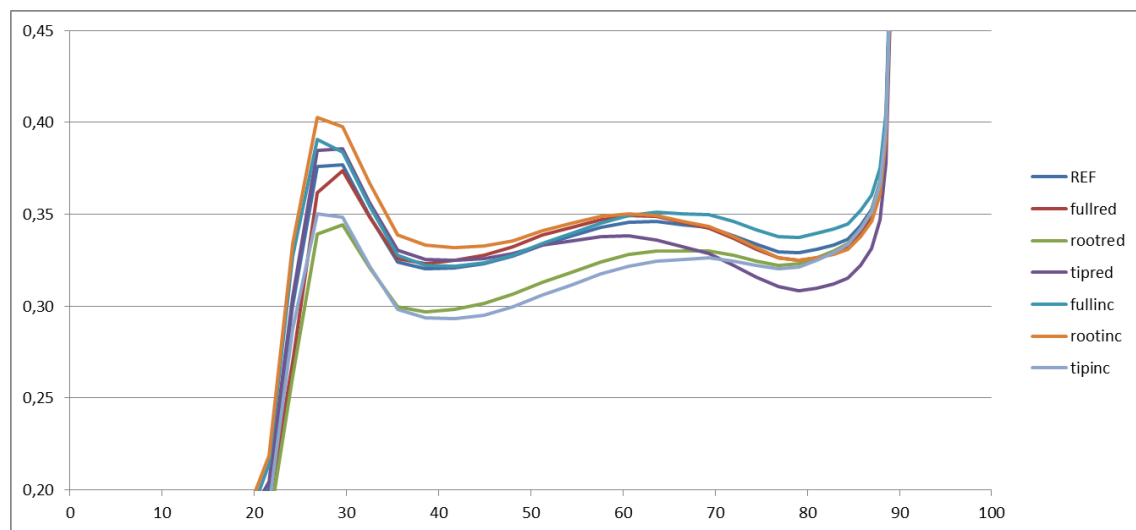


Figure 36 The axial induction distribution along the blade span for a 10% change in chord

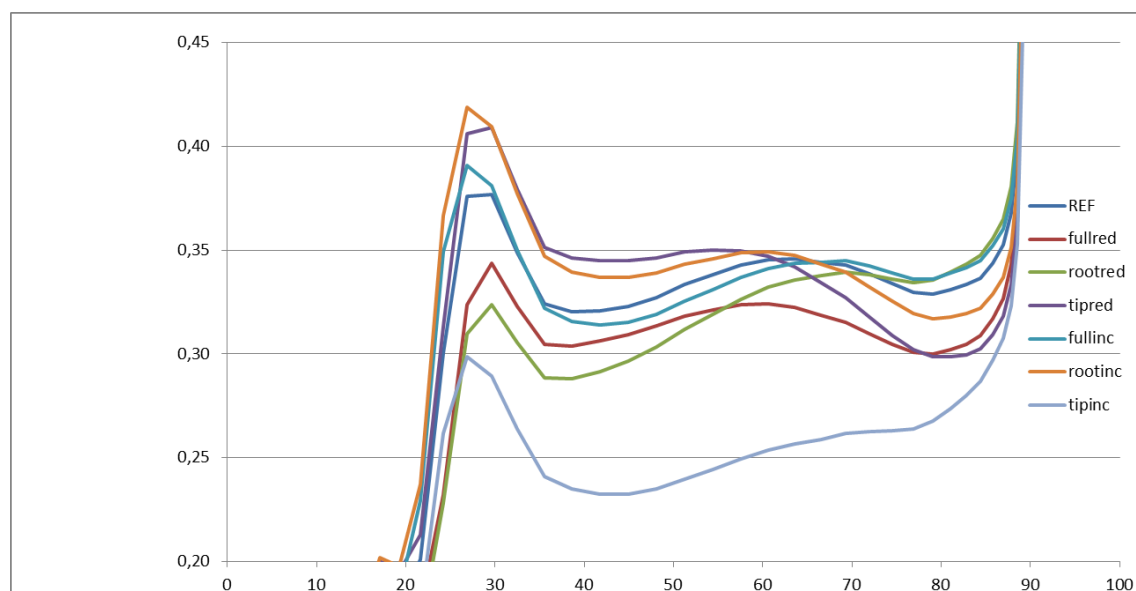


Figure 37 The axial induction distribution along the blade span for a 20% change in chord

The resulting power and thrust curves are slightly different but the difference is too small to show in a graph. Therefore the energy yield for the reference wind speed distribution is shown in Table 7 and Table 8. The thrust curve shows larger deviations from the reference design, however it is

chosen to show the difference in the thrust coefficient C_T at 9 m/s due to the fact that that is a good indication for the changes in wake effects. The lower the thrust curve or coefficient at 9 m/s the lower the wake effects when the wind turbine is installed in a larger array of wind turbines.

Table 7. Relative changes in yield, blade and tower weight and the resulting LCoE for the 10% change in chord distributions

	Ref.	Full Red.	Root Red	Tip-Red.	Full Inc.	Root Inc.	Tip Inc.
Yield	100,00%	100,01%	99,94%	99,79%	99,60%	99,77%	99,66%
C_T @ 9 m/s	100,00%	99,71%	97,35%	98,41%	101,10%	100,72%	97,05%
Blade weight	100,00%	108,70%	108,67%	98,95%	96,25%	93,98%	101,95%
Tower weight	100,00%	97,84%	97,84%	97,84%	102,25%	102,25%	97,84%
LCoE [€/MWh]	91,93	92,11	92,17	91,95	92,29	92,06	92,17

Table 8. Relative changes in yield, blade and tower weight and the resulting LCoE for the 20% change in chord distributions

	Ref.	Full Red.	Root Red	Tip-Red.	Full Inc.	Root Inc.	Tip Inc.
Yield	100,00%	99,91%	99,93%	99,72%	99,63%	99,61%	97,96%
C_T @ 9 m/s	100,00%	95,40%	97,64%	98,87%	100,61%	100,62%	85,06%
Blade weight	100,00%	111,65%	121,05%	98,26%	93,43%	89,35%	104,19%
Tower weight	100,00%	91,87%	97,84%	97,84%	107,04%	102,25%	102,25%
LCoE [€/MWh]	91,93	91,89	92,64	91,98	92,46	92,03	94,09

3.4 Conclusions

The analysis shows that the influence of the different axial induction distribution on the LCoE is not very high. There is not an obvious winner, the 20% full reduction has a very small advantage on the reference but it is assumed that this difference is well within the accuracy of the analysis.

It would be possible to reduce the tower top weight, the highest decrease would be for the 20% increase of the root, but the integral analysis however does not show that this would result in a substantial lower LCoE, actual due to the fact that the tower would become more expensive and a slightly lower yield resulted in a slightly higher LCoE.

The result is that by reducing the chord distribution, especially for the full reduction of both 10 and 20% results in substantially higher blade weights. This is caused due to the fact that by reducing the chord also the thickness of the section is reduced which has a high influence on the required skin thickness and consequently on the weight. Reducing only the tip and not the root has a beneficial effect on the weight of the blades.

The tower model also showed some surprising results, due to frequency restrictions the model quit often ended up with the same dimensions resulting in equal weight and thus cost.

In this study it was chosen not to optimise the twist and thickness distribution for the different chord distribution due to the fact that it would then not be fair to compare it with the reference model any more.

The difference in thrust coefficient is not used in the final analysis. The concepts that have a low thrust coefficient will actually have lower wake effects and that will decrease the LCoE for the 20

full reduction design that has a decrease in LCoE, although very minimal of € 0,04 / MWh but also has a thrust coefficient that is 4.6% lower than the reference design.

References

- [1] Kirby Ch., S. Calverley, E. Stehouwer, and H.B. Hendriks, "Front-mounted magnetically-g geared pseudo direct drive generator," *WindTech Magazine*, vol. vol. 10, October 2014.
- [2] Abrahamsen A. B., N. Magnusson, D. Liu, E. Stehouwer, H.B. Hendriks, and H. Polinder, "Design study of a 10 MW MgB2 superconductor direct drive wind turbine generator," in *Proceedings of the EWEA Conference Barcelona, 2014*.
- [3] Altair Engineering Inc., *HyperMesh Desktop Introduction Pre-processing for Finite Element Analysis*, 2014.
- [4] Altair Engineering Inc., *OptiStruct for Structural Optimization Including Concept Methodologies and Optimization Examples*, 2014.
- [5] C. Bak, F. Zahle, R. Bitsche, T. Kim, A. Yde, L. Henriksen, P. Andersen, A. Natarajan, and M. Hansen, "Description of the dtu 10 mw reference wind turbine," Report I 0092, DTU Wind Energy, Risø Campus, Roskilde, Denmark, July 2013. To be accepted.
- [6] "Guideline for the certification of wind turbines," 2010.
- [7] D. Ancona and McVeigh, "Wind turbine - materials and manufacturing fact sheet," 2001.
- [8] D. R. Wilburn, "Wind energy in the united states and materials required for the land-based wind turbine industry from 2010 through 2030," Scientific Investigations Report 2011-5036, U.S. Geological Survey, Reston, Virginia, 2011.
- [9] <http://www.iron foundry.com/>, May 2015.
- [10] <http://www.sn castiron.nl/>, July 2015.
- [11] Windtec Solutions, "Seatitan? 10 MW Wind Turbine," July 2015.
- [12] R. van Hoof, "Topological optimization of a wind turbine main frame," Tech. Rep. MEC-08140, Mecal, MECAL, Enschede, the Netherlands, June 2011.
- [13] H. Niemann, "A simple topology optimization example with md r2 patran," tech. rep., University of Toulouse and Institut of Aircraft Design and Lightweight Structures, 2008.
- [14] C. Wook-han, H. Cheng-guo, K. Jong-moon, and P. Gyung-Jin, "Comparison of some commercial software systems for structural optimization," in *11th World Congress on Structural and Multidisciplinary Optimisation*, June 2015.
- [15] C. Fleury and V. Braibant, "Structural optimization: a new dual method using mixed variables," *International Journal for Numerical Methods In Engineering*, vol. Vol. 23, pp. 409–428, 1986.
- [16] J. Montgomery, "Methods for modeling bolts in the bolted joint," in *ANSYS User's Conference*, 2002.
- [17] *Guidelines for Design of Wind Turbines*. Denmark: DNV/Risø, 2002.
- [18] S. R. Harichandran and A. H. Varma, "Design of steel structures; chapter 5: Design of bolted connections." <http://www.egr.msu.edu/harichan/classes/ce405/>.
- [19] G. Sieros, P. Chaviaropoulos, J. Sørensen, B. Bulder, and P. Jamieson, "Upscaling wind turbines: theoretical and practical aspects and their impact on the cost of energy," *Wind Energy*, vol. 15, pp. 3–17, 2012.
- [20] E. Bot and O. Ceyhan, *Blade Optimization Tool User Manual; ECN-E-09-092*. ECN, Petten, December 2009.

Appendix A Concept design of 10 MW direct drive wind turbine after mass reduction

